Superconducting R&D

Magnet System Department

Fermilab Technical Division

Parametric Study of Mechanical Behavior of Superconducting Solenoids

Author Giacomo Ragni

.....

Supervisor Emanuela Barzi

.....

Contents

1 Analytical model **1**

1.1 Magnetic model 1

1.1.1 Engineering Current Density 1

1.1.2 Analytic expressions of magnetic field 3

1.1.3 Self-field configuration 5

1.1.4 Insert coil configuration 7

1.2 Mechanical model 7

1.2.1 Determination of the Young modulus 8

1.2.2 Planar stresses 9

1.2.3 Axial stress 10

1.3 Thermal model 11

1.3.1 Skin with rigid boundary conditions 11

1.3.2 Coil and skin unloaded 12

1.4 Effects of interference 12

1.5 Effects of winding coil 15

1.6 Analytical model of the superconductor 16

2 Validation of the analytical model **17**

2.1 Finite Elements Method Analysis 17

2.2 Study of the mid plane 18

2.3 Results 18
2.3.1 Self-field configuration 19
2.3.2 Insert coil with 10 T outer field 19
2.3.3 Insert coil with 20 T outer field 22
2.4 Comparion with the previous model 22

3 Parametric analysis 27
3.1 Sensitivity to physical constants 27
3.2 Effect of magnetic field 27
3.2.1 Self field configuration 27
3.2.2 Insert coil configuration 29
3.3 Effects of geometric parameters 32
3.4 Winding coil and assembly interference 33
3.4.1 Interference 33
3.4.2 Winding coil 33
3.4.3 Combination of effects 33

4 Multiple skins configuration 38
4.1 Analytical model 38
4.2 Results 39
4.3 Sensitivity to physical parameters 39
4.3.1 Magnetic field 39
4.3.2 Geometrical optimization 41
4.4 Discussion 43

5 Applications of the analytic cal model 44
5.0.1 Estimate of the preload force 44
5.0.2 Estimate of the winding force 44

6 Case studies **45**

6.1 National High Magnetic Field Laboratory 45

6.1.1 Geometry 45

6.1.2 Critical current 45

6.1.3 Results 45

6.2 Massachusetts Institute of Technologies 45

6.2.1 Geometry 47

6.2.2 Results 47

6.3 Brookhaven National Laboratory 47

6.3.1 Geometry 47

6.3.2 Results 47

Bibliography **51**

A Definition of the standard solenoid **53**

A.1 Double coil 53

B Materials properties **54**

C Mathcad code **56**

List of Figures

1.1 Engineering current density 2
1.2 Distribution of axial field in a section of the coil 4
1.3 Distribution of self-field in the coil 4
1.4 Distribution of radial field in a section of the coil 5
1.5 Distribution of radial field in a section of the coil 6
1.6 Magnetic self-field distribution 7
1.7 Magnetic field distribution in an insert coil configuration . . . 8
1.8 Geometry of the elementary cell of the coil 8
1.9 Stresses due to a $0.05mm$ interference 13
1.10 Effects of interferences and thermal contraction 14
1.11 Stresses due to winding coil 15

2.1 Stress intensity 18
2.2 Stress distribution along the axis 19
2.3 Stresses in a self field solenoid 20
2.4 Detailed stresses in the self field solenoid 21
2.5 Stresses in an insert coil solenoid 22
2.6 Planar stresses in the insert coil solenoid (10 T) 23
2.7 Stresses in an insert coil solenoid 24
2.8 Planar stresses in the insert coil solenoid (20 T) 25

2.9 Detailed stresses in the self field solenoid 26

3.1 Sensitivity to physical parameters 28
3.2 Outer radius 29
3.3 Stresses in the solenoid 30
3.4 Outer radius in the insert coil 30
3.5 Hoop stresses in the insert coil 31
3.6 Effects of the skin thickness 33
3.7 Effects of interference on stresses at the assembly condition . . 34
3.8 Effects of interference on stresses at the working condition . . 35
3.9 Effects of winding coil on stresses at the working condition . . 36
3.10 Hoop stres in the coil due to interference and winding 37

4.1 Stress comparison 39
4.2 Maximum hoop stresses depending on the Young modulus of the inner skin 40
4.3 Total self-field depending on R_m 41
4.4 Outer radius 42
4.5 Optimized geometry 42

6.1 Critical current 46
6.2 Stress in NHMFL coil 46
6.3 Stress in MIT coil 48
6.4 Stress in MIT coil 48
6.5 Stresses without pre-stress 50

List of Tables

1.1 Properties of the elementary cell 9

3.1 Self-field configurations 32
3.2 Insert coil configurations 32

6.1 National High Magnetic Field Laboratory coil geometry 47
6.2 MIT insert 1 47
6.3 MIT insert 2 49
6.4 Brookhaven insert 1 49
6.5 Brookhaven insert 2 49
6.6 Self-field configurations 49

B.1 Coefficients of thermal dilatation 55

Chapter 1

Analytical model

The parametric study of superconducting solenoids was performed exploiting a full analytical model made of two different submodels:

- the magnetic model describes the radial and axial magnetic fields and the current density in the coil
- the mechanical model describes the stresses due to the forces caused by the magnetic fields and mechanical constraints.

In the next section these models are described more in detail.

1.1 Magnetic model

Before performing any mechanical calculation it is necessary to evaluate the effects of the magnetic fields on the structure of the solenoid. In fact, because of the Lorentz's force, if the superconductor has a current, it is loaded with a force described as

$$\vec{F} = \int \vec{J} \times \vec{B} \tag{1.1}$$

It is important to determine the relationships between the current density, the magnetic fields and the geometry of the coil.

1.1.1 Engineering Current Density

The Engineering Current Density represents the limit for the current density in the coil that can't be exceeded [4]. It has been defined as a function of the total magnetic field in the solenoid. It has been determined fitting experimental results and its analytical expression is

$$J_c = c_1 e^{-c_2 B} + c_3 e^{-c_4 B} \tag{1.2}$$

where the coefficients at 95% confidence level have the following values:

$$c_1 = 1018$$

$$c_2 = 0.3606$$

$$c_3 = 503.3$$

$$c_4 = 0.01702$$

Figure 1.1 shows the Engineering Current Density curve.

1.1.2 Analytic expressions of magnetic field

The object of this study is a thick and finite-length solenoid [5], so we can define the azimuthal component of vector potential as

$$A_\phi(r,z) = \frac{\mu_0}{4\pi} J(B) \int_{-\frac{L_c}{2}}^{\frac{L_c}{2}} \int_{R_1}^{R_2} a \int_0^{2\pi} \frac{cos(\theta)}{\sqrt{(z-l)^2 + r^2 + a^2 - 2arcos(\theta)}} d\theta \, da \, dl \tag{1.3}$$

As a consequence of that the two components of the magnetic field (axial and radial) are respectively

$$B_z(r,z) = -\frac{1}{r} \frac{\partial \left[r A_\phi(r,z) \right]}{\partial r} \tag{1.4}$$

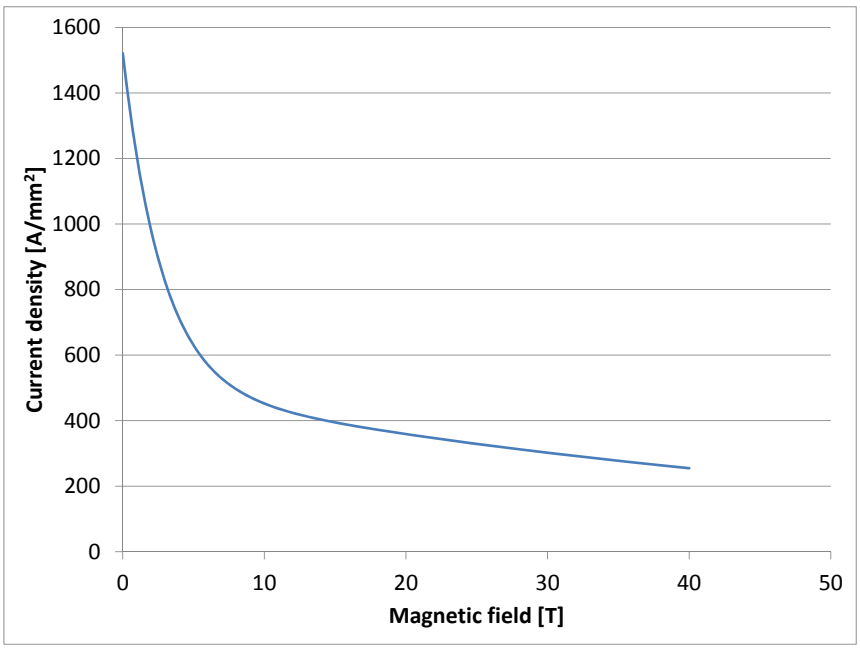

Figure 1.1: Engineering current density

$$B_r(r,z) = -\frac{\partial A_\phi(r,z)}{\partial z} \tag{1.5}$$

Because of the Lorentz's force, described in Equation 1.1, the axial magnetic field creates radial forces, while the radial field creates an axial force, which is often neglected.

The main component of the magnetic field is the axial one. It is maximum at the mid-plane and at the inner radius, as shown in Figure 1.2, while it resets to zero at the outer border. For future calculations it is assumed to be constant along the axial length and be linear along the radius.

Looking at the plot in Figure 1.3, it is obvious that this approximation of considering linear the distribution of the magnetic field is perfectly acceptable. The bullets in blue are the results obtained with the analytic expression 1.4.

The radial component distribution of the magnetic field is shown in Figure

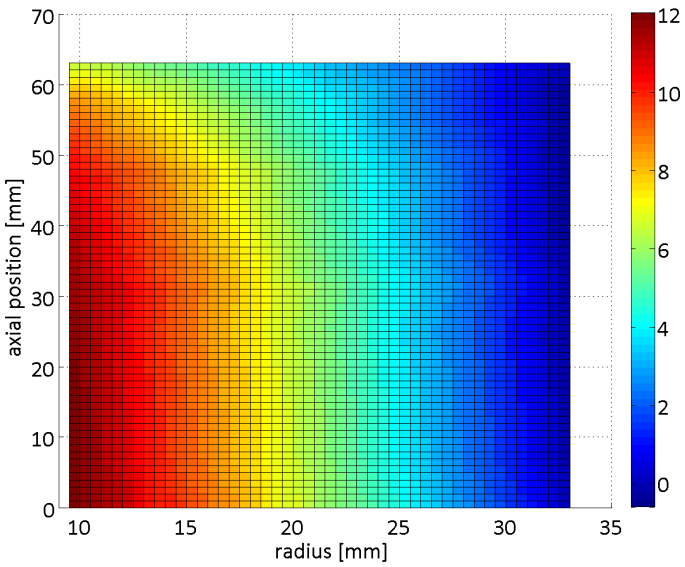

Figure 1.2: Distribution of axial field in a section of the coil

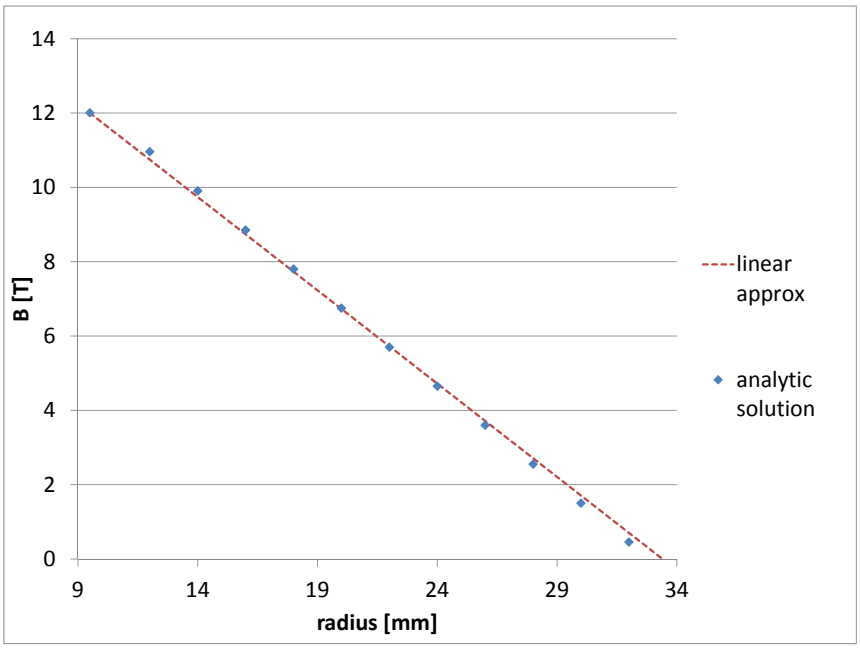

Figure 1.3: Distribution of self-field in the coil

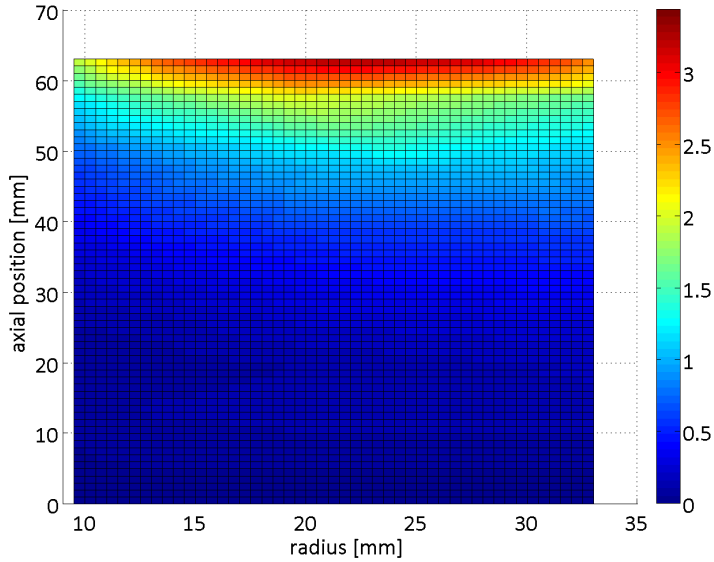

Figure 1.4: Distribution of radial field in a section of the coil

1.4. On the contrary of the axial one, it is maximum and the axial border and it decreases coming up to the mid-plane.

In order to estimate the mechanical effects of the radial component of the magnetic field it has been considered to have a quadratic behavior along the axial length. The resulting error is little percentage, but it is precautionary because it overestimates the real distribution, as show in Figure 1.5.

In the future, when speaking about self-field we are considering the axial component.

1.1.3 Self-field configuration

The magnetic field created by the solenoid itself if loaded by an electric current depends on a number of geometric parameters. In particular, if the hypothesis of infinite length is done, the magnetic field can be obtained with

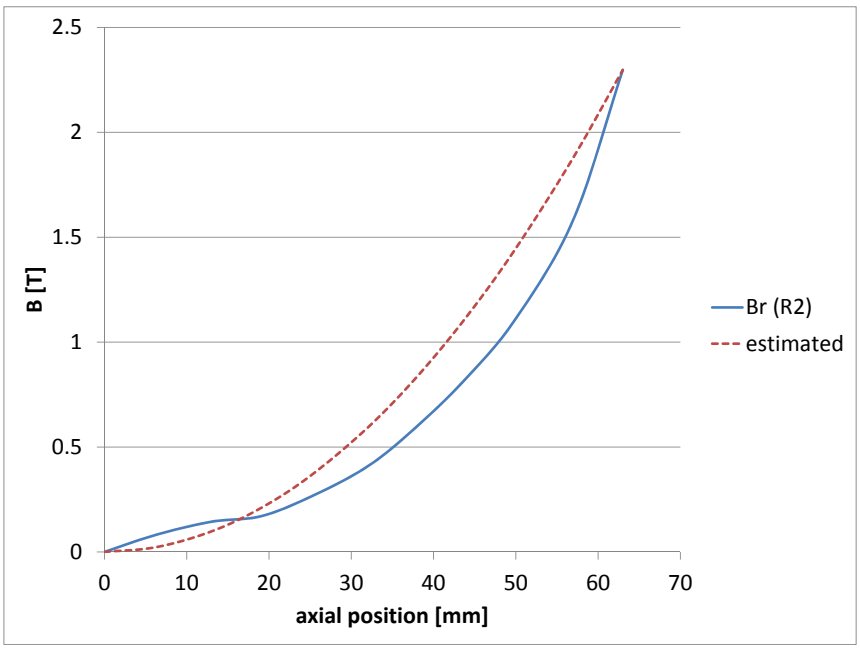

Figure 1.5: Distribution of radial field in a section of the coil

a simplified expression [12]

$$B_\infty(\alpha) = R_1(\alpha - 1)\mu_0 J \tag{1.6}$$

If the length of the coil is L_c, the maximum magnetic field B_0 is

$$B_0(\alpha, \beta) = R_1\mu_0 J\beta ln\left(\frac{\sqrt{\alpha^2+\beta^2}+\alpha}{\sqrt{1+\beta^2}+1}\right) \tag{1.7}$$

where $\alpha = \frac{R_2}{R_1}$ and $\beta = \frac{L_c}{2}\frac{1}{R_1}$

In order to calculate the forces in all the solenoid, the hypothesis of a linear distribution of magnetic field has been made as shown in the following equation and in Figure 1.6.

$$B_0(r) = \begin{cases} B_0 & if\ r < R_1 \\ B_0\left(1 - \frac{r-R_1}{R_2-R_1}\right) & if\ r \geq R_1 \end{cases}$$

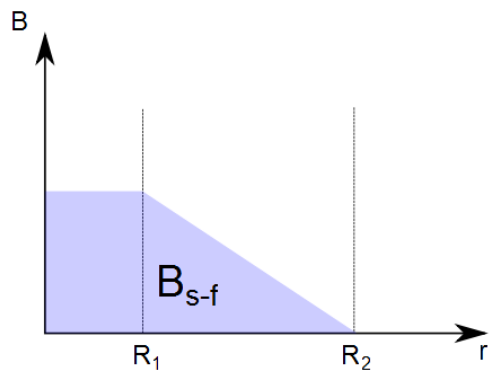

Figure 1.6: Magnetic self-field distribution

1.1.4 Insert coil configuration

In this new configuration the self-field and the background field are overlapped and this last is considered to be constant in all the coil [7]. The distribution of the magnetic field is shown in Figure 1.7

1.2 Mechanical model

Starting from the results obtained by the magnetic analysis and considering the mechanical effects due to the Lorentz force of Equation 1.1, the mechanical behavior of the superconducting solenoid was modeled taking into account the two different parts comprised in the structure: coil and steel skin.

The first approach was very simple: only planar stresses were considered because hoop stress is the first principal one and is far bigger than the others, radial and axial. Then the axial component was introduced using a beam model and finally, these results were coupled and the mechanical effects were superposed.

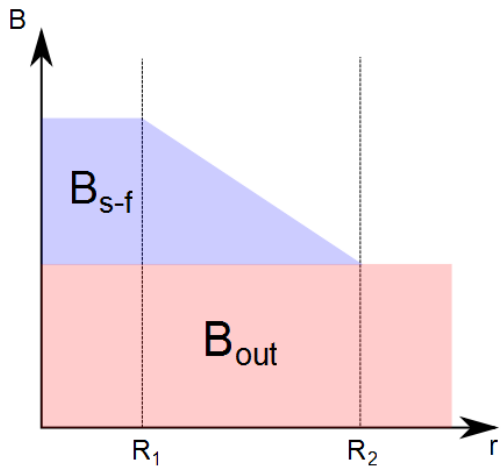

Figure 1.7: Magnetic field distribution in an insert coil configuration

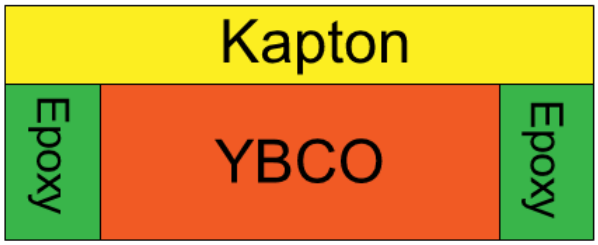

Figure 1.8: Geometry of the elementary cell of the coil

1.2.1 Determination of the Young modulus

The superconductor is actually composed of three different materials as shown in Figure 1.8.

To calculate the Young modulus for the analytical model the areas of the different materials were considered and an averaged modulus was chosen, using the data in 1.1.

Material	E (MPa)	area (mm^2)
YBCO	110	0.4
Kapton	5.5	0.1125
Epoxy	4.5	0.05

Table 1.1: Properties of the elementary cell

1.2.2 Planar stresses

Exploiting the axial symmetry of loads and geometry of the problem, it can be solved using Lamé's equation [10, 13], which is able to describe both the coil and the skin.

$$\frac{E}{1-\nu^2}\left(\frac{d^2u}{dr^2}-\frac{1}{r}\frac{du}{dr}-\frac{u}{r^2}\right)+f=0 \tag{1.8}$$

In the two different magnetic configurations studied the following f was used.

$$f = J \cdot B(r) \qquad \text{self field}$$

$$f = J \cdot (B(r) + B_{out}) \qquad \text{insert coil}$$

where

$$B(r) \quad \begin{cases} B_0 & if\ r < R_1 \\ B_0(1-\frac{r-R_1}{R_2-R_1}) & if\ r \geq R_1 \end{cases}$$

The steel skin was supposed to be unloaded so in its equation it is always $f = 0$

The four coefficients can be determined imposing the boundary conditions on the free surface and at the interface between coil and skin.

$$\sigma_{rr,c}(R_1) = 0$$
$$\sigma_{rr,s}(R_2 + t) = 0$$
$$\sigma_{rr,c}(R_2) - \sigma_{rr,s}(R_2) = 0$$
$$u_{c_2}(R_2) - u_{s_2}(R_2) = 0$$

Imposing a plane stress hypothesis, it is very simple to determine deformations

$$\epsilon_{rr}(r) = \frac{du}{dr}$$
$$\epsilon_{\theta\theta}(r) = \frac{u}{r}$$

and stresses

$$\sigma_{rr}(r) = \frac{E}{1-\nu^2}\left[\epsilon_{rr}(r) + \nu\epsilon_{\theta\theta}(r)\right]$$
$$\sigma_{\theta\theta}(r) = \frac{E}{1-\nu^2}\left[\epsilon_{\theta\theta}(r) + \nu\epsilon_{rr}(r)\right]$$

1.2.3 Axial stress

One of the tasks was the modeling of axial forces which are usually neglected in analitical studies. First of all the congruence of axial deformations was imposed. In particular, if we consider the mid-plane section of the coil, the deformation along the radius must be constant. If axial forces are imposed equal to zero, the deformation must be zero all along the radius, so:

$$\epsilon_{zz}(r) = \frac{\sigma_{zz}(r)}{E} - \frac{\nu}{E}\left(\sigma_{rr}(r) + \sigma_{\theta\theta}(r)\right) = 0 \tag{1.9}$$

and

sistemare

Then, if we consider known the total axial force in one half of the coil, the resultant stress in the mid-plane section is:

$$\sigma_{zz_{magnetic}} = \frac{F_{axial}}{\pi \left(R_2^2 - R_1^2\right)} \tag{1.10}$$

where $F_{axial} = B_r I \pi \left(R_1 + R_2\right)$

This expression can be obtained analyzing the coil with the beam model and considering it loaded only with an axial force.

At the end the total axial stress is

$$\sigma_{zz}(r) = \sigma_{zz_{congruence}}(r) - \bar{\sigma}_{zz_{congruence}} + \sigma_{zz_{magnetic}} \tag{1.11}$$

1.3 Thermal model

The effects of temperature in a cryogenic environment cannot be neglected, so an analytical description of the thermal effects on the superconductor was developed.

In axial symmetrical plates the general equation to describe thermal stresses is [10]:

$$\begin{pmatrix} \sigma_{rr} \\ \sigma_{\theta\theta} \end{pmatrix} = \frac{E}{1-\nu^2} \begin{pmatrix} 1 & \nu \\ \nu & 1 \end{pmatrix} \begin{pmatrix} \epsilon_{rr} - \alpha\Delta T \\ \epsilon_{\theta\theta} - \alpha\Delta T \end{pmatrix} = \frac{E}{1-\nu^2} \begin{pmatrix} 1 & \nu \\ \nu & 1 \end{pmatrix} \begin{pmatrix} \frac{du}{dr} - \alpha\Delta T \\ \frac{u}{r} - \alpha\Delta T \end{pmatrix} \tag{1.12}$$

Both coil and skin have the same constant temperature ($4.2K$), so all the stresses are caused by the different coefficients of thermal dilatation of the steel and of the superconductor. In analytical calculations the coefficients of thermal dilatation were supposed to be $8 \cdot 10^{-6} K^{-1}$ for the coil and $10 \cdot 10^{-6} K^{-1}$ for the skin , while more detailed data are in the Appendix B.

In order to verify the accuracy of the model and the correctness of the code implemented on MathCad some simple cases were analyzed and the distributions obtained confirmed the coherence with the theory.

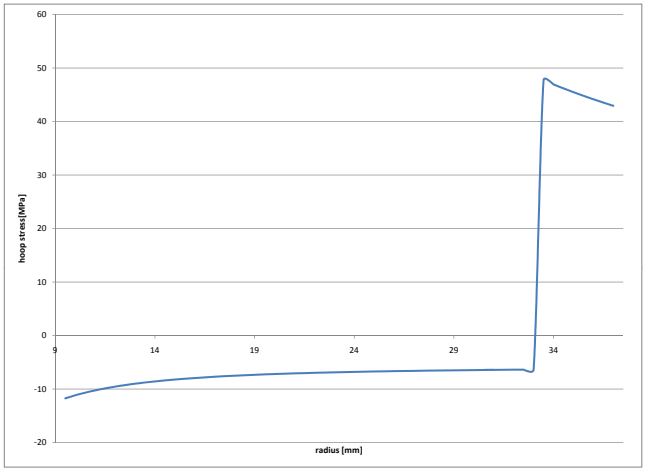

(a) Hoop stress

5interference_radial.pdf

(b) Radial stress

Figure 1.9: Stresses due to a $0.05mm$ interference

1.4 Effects of interference

In order to reduce the maximum hoop stress on the coil it is possible to assembly the skin with a small interference. In this case the skin has an higher stiffness, so its maximum stress increases. It is important to solve the trade off between this two effects to avoid the skin exceed the elastic limit. In order to better understand these effect, in Figure 1.9 the hoop and radial stresses of the standard solenoid unloaded with an assembly interference of $0.05mm$ are shown.

In Figure 1.10 there are the hoop stresses, the most important for resistance considerations, due to different interferences and to the thermal effect of cooling in an unloaded coil. Actually they seem to have the same ef-

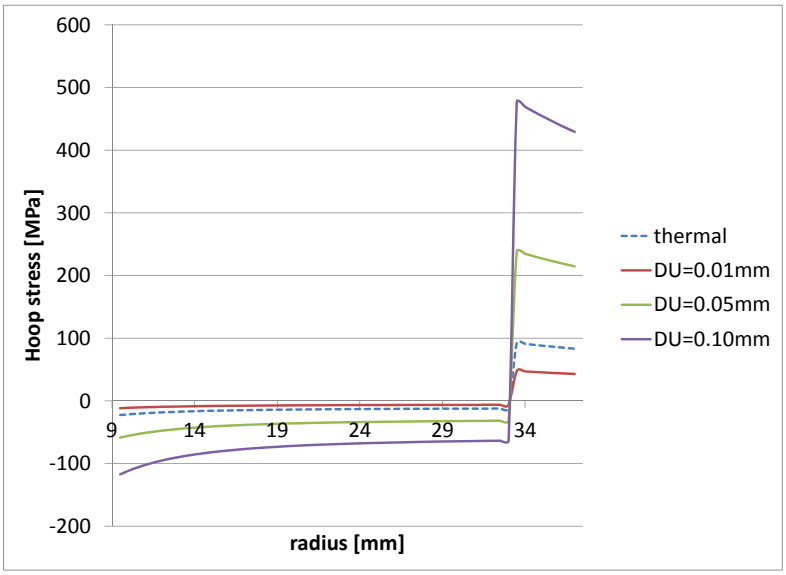

Figure 1.10: Effects of interferences and thermal contraction

fects, so they can be combined to modify the maximum hoop stresses and, in particular to reduced the hoop stress at the inner radius of the coil.

To obtain the analytic solution of this problem the principle of superposition of the effects have been exploited. First of all, the equation 1.8 has been resolved only for the skin simply imposing

$$f = 0$$

$$u(R_2) = \Delta U$$

$$\sigma_{rr}(R_2 + t) = 0$$

Then this solution was superposed to the standard one and all the stresses were calculated.

5winding_hoop.pdf

(a) hoop stress

5winding_radial.pdf

(b) hoop stress

Figure 1.11: Stresses due to winding coil

1.5 Effects of winding coil

The superconductor is usually made of ropes, so it is possible to mount them preloaded in order to modify their mechanical behavior during the working. As for the coil it is possible to estimate the effect of an assembly interference on the stresses, supposing to have a smaller coil and constraining it to stay out of a rigid cylinder.

In Figure 1.11 are shown the stresses due to a radial displacement of the inner radius of the coil of $0.05mm$. As for the interference, the effect of the winding coil was obtained imposing a fixed displacement at the inner radius of the coil and superposing the effects of all the loading conditions.

Considering the manufacturing process of the winding coil, the following boundary conditions were imposed to solve the homogeneous differential

equation 1.8

$$u(R_1) = W_{coil}$$
$$\sigma_{rr}(R_2) = 0$$

As shown in Figures 1.9 and 1.11, the assembly interference and the winding coil seem to have opposite effects on the stresses of the two components of the solenoid. The interference increases stresses on the skin, while the winding coil increases the coil stresses. Actually, both of them increase the stiffness of the structure reducing the maximum axial displacement of the coil, but they split the necessary stresses in different ways.

1.6 Analytical model of the superconductor

Finally a complete analytical description of the mechanical behavior of the superconductor was developed, in order to describe displacements and stresses of both the components, coil and skin.

The model is simplified considering the superconductor an homogeneous and isotropic material, but the results found are not far from those obtained with a mesomechanical and anisotropic model realized in ANSYS. The main advantages of this new model are the possibility to make studies of all the parameters involved in the problem and the great decrease in calculations time.

Chapter 2

Validation of the analytical model

The results obtained by the analytical model of the solenoid were compared with the results obtained by simulations of a mesomechanic model in ANSYS [1]. In order to verify all the hypothesis made, three different configurations of the same solenoid were considered. In particular a standard solenoid was defined (more details in the Appendix A) to perform all the parametric studies with the same geometry.

2.1 Finite Elements Method Analysis

Because of the detailed modeling of the mesomechanic model, it was considered as a benchmark for our analytical model, even if in this too some simplifying hypothesis have been made. To solve computational problems the contact between the superconducting coil and the steel skin was considered as a *glued connection* while actually it is a contact with friction and sliding surfaces are allowed.

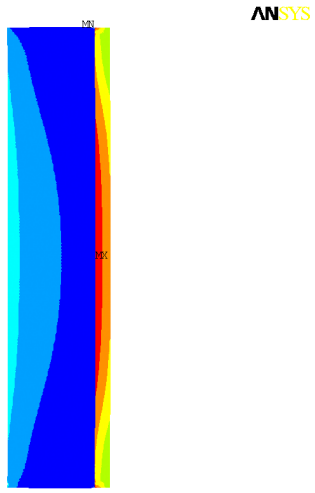

Figure 2.1: Stress intensity

2.2 Study of the mid plane

In the analytic model only the mid plane of the solenoid was considered, under the reasonable hypothesis that it was the most stressed. Actually, using ANSYS, it is very simple to verify this hypothesis to be fully true. Figure 2.1 shows the contour plot of stress intensity obtained by ANSYS nodal solution and in Figure 2.2 there are the distributions of stresses for the coil at R_1 and for the skin at R_2.

In the future plots only the mid plane stresses will be considered because it is the most critical for resistance considerations.

2.3 Results

In this section it is possible to see all the three principal stresses in the coil and in the skin of the three configurations studied:

- standard solenoid in self field ($12T$)

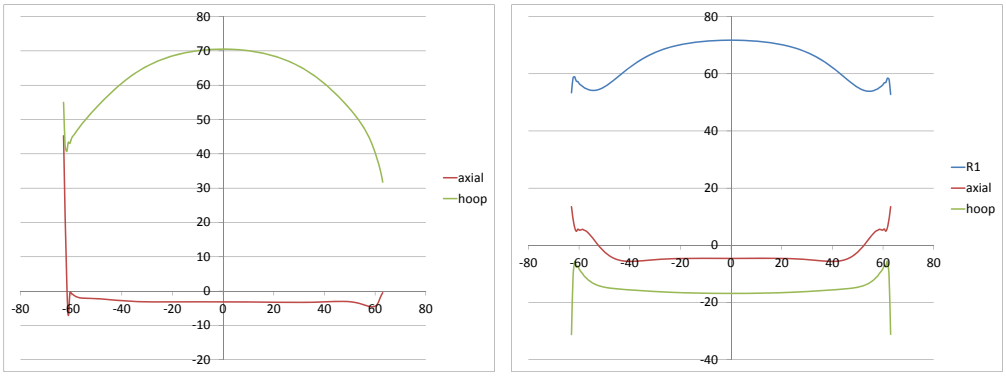

(a) stresses on the coil (b) stresses on the skin

Figure 2.2: Stress distribution along the axis

- insert coil standard solenoid with $10T$ background field
- insert coil standard solenoid with $20T$ background field

2.3.1 Self-field configuration

In Figure 2.3 there are the distributions along the radius of the three components of the stresses obtained with the analitic solution. It is very easy to realize that for resistance considerations, the hoop stress is the most important, both for coil and skin.

More in detail, in Figure 2.4, there are the comparisons among the results obtained by the two models used.

TABELLA CON ERRORI ???

2.3.2 Insert coil with 10 T outer field

In Figure **??** there are the distributions along the radius of the three components of the stresses in the two different models.

More in detail, in Figure 2.6, there are the comparisons among the results

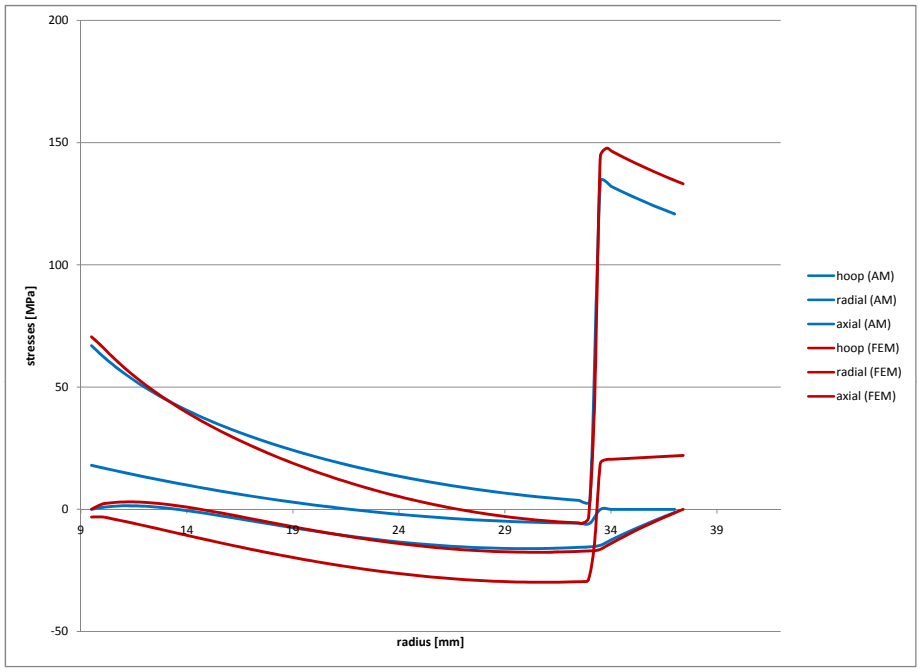

Figure 2.3: Stresses in a self field solenoid

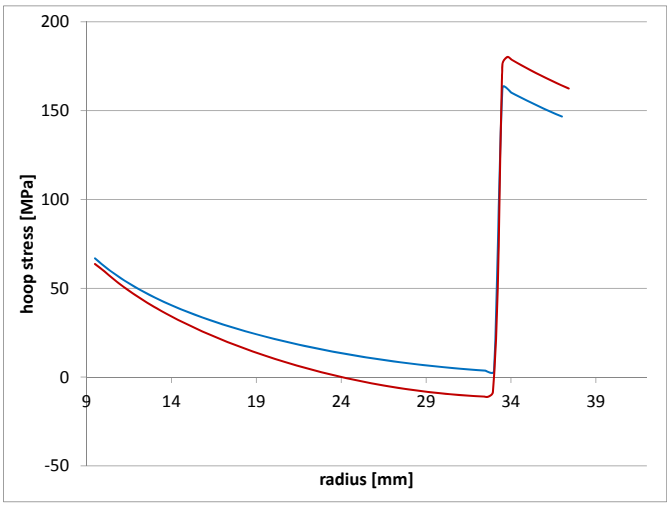

(a) hoop stress

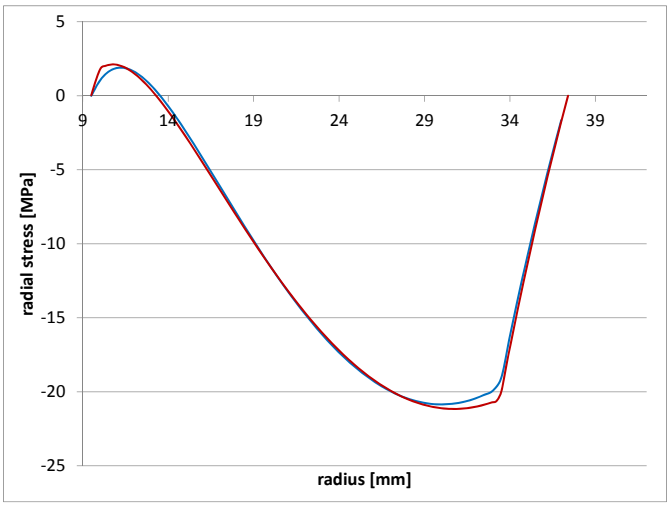

(b) radial stress

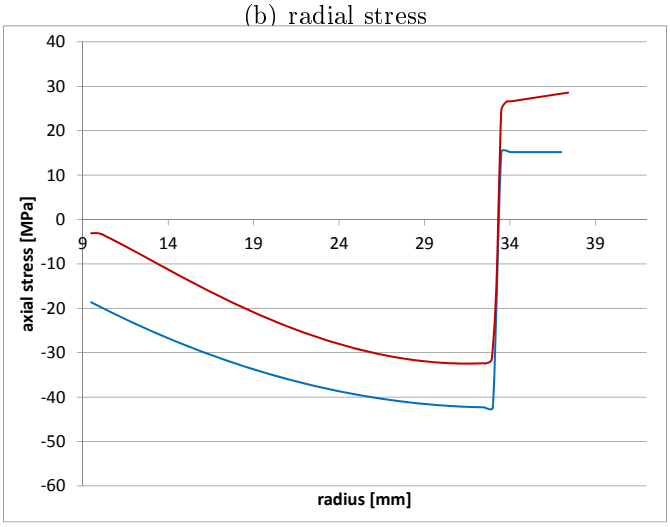

(c) axial stress

Figure 2.4: Detailed stresses in the self field solenoid

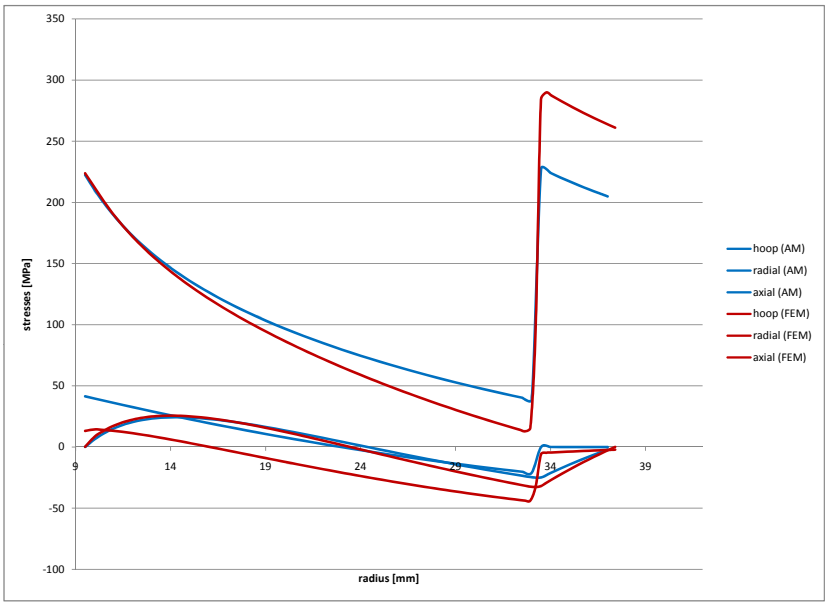

Figure 2.5: Stresses in an insert coil solenoid

obtained by the two models used

TABELLA CON ERRORI ???

2.3.3 Insert coil with 20 T outer field

In Figure 2.7 there are the distributions along the radius of the three components of the stresses in the two different models.

More in detail, in Figure 2.8, there are the comparisons among the results obtained by the two models used

TABELLA CON ERRORI ???

2.4 Comparion with the previous model

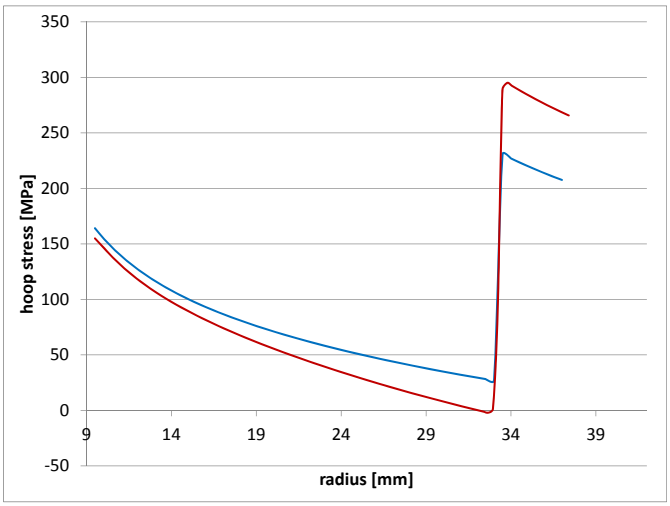

(a) hoop stress

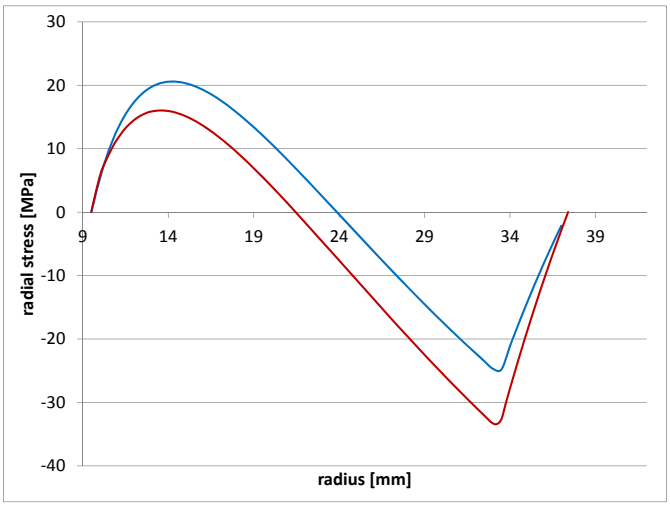

(b) radial stress

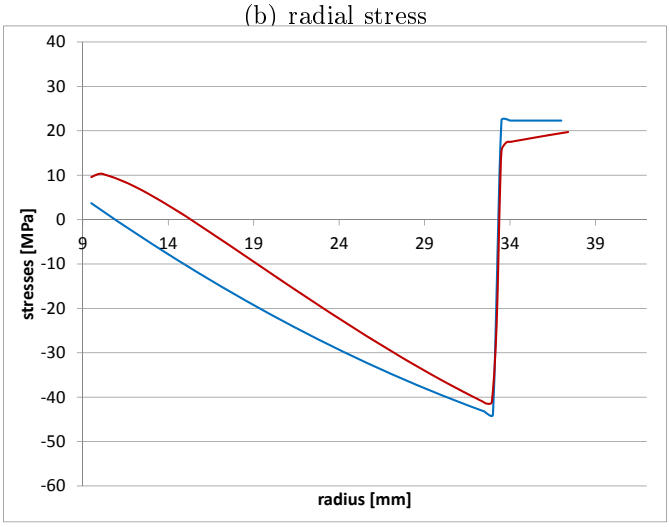

(c) axial stress

Figure 2.6: Planar stresses in the insert coil solenoid (10 T)

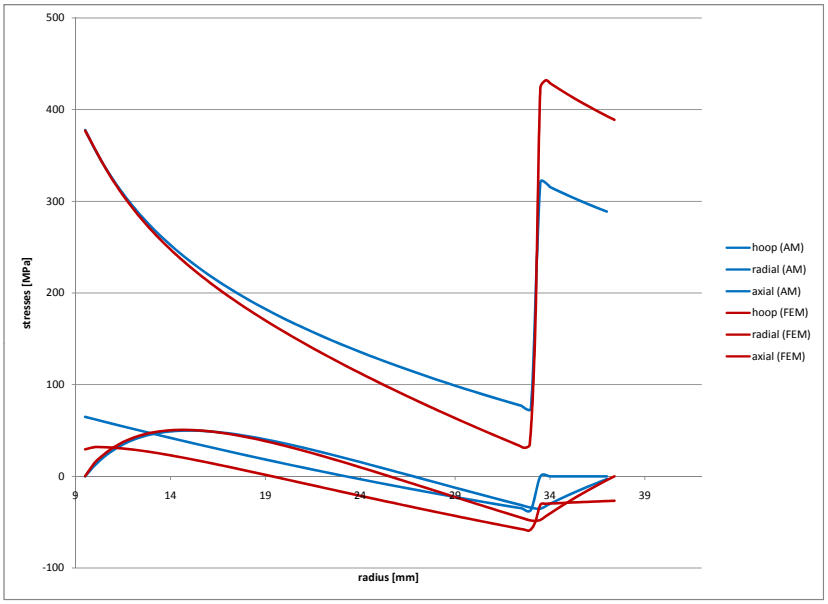

Figure 2.7: Stresses in an insert coil solenoid

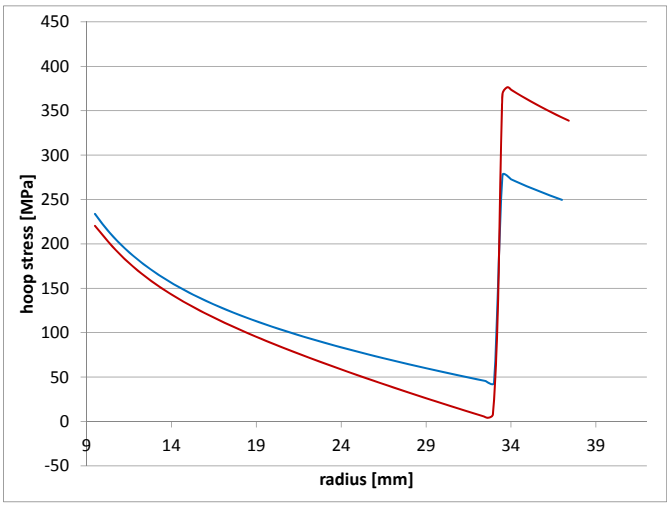

(a) hoop stress

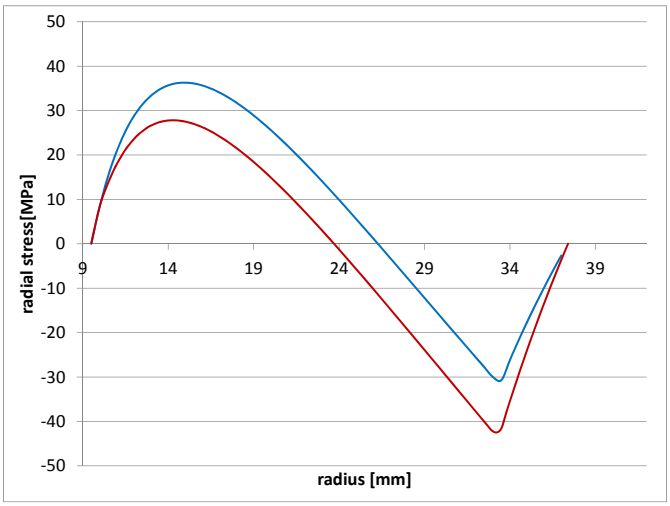

(b) radial stress

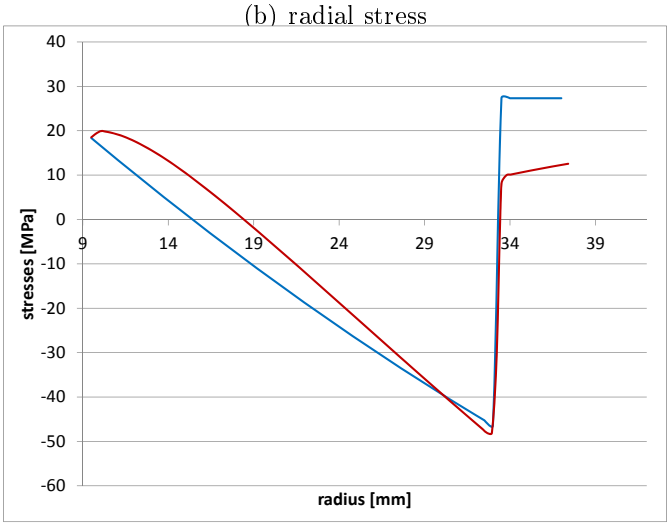

(c) axial stress

Figure 2.8: Planar stresses in the insert coil solenoid (20 T)

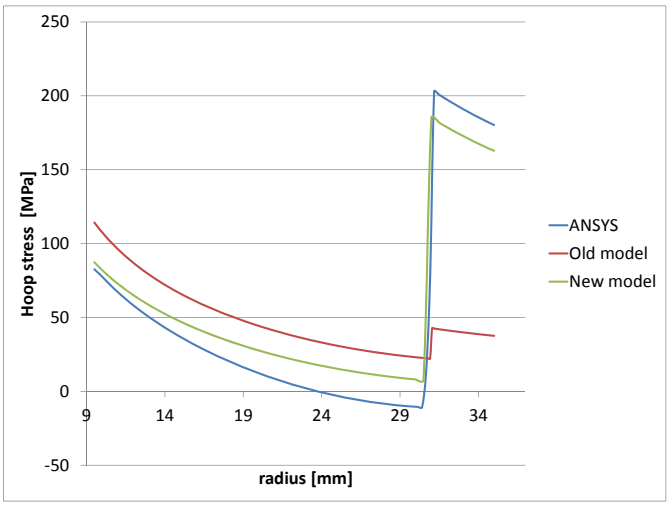

(a) hoop stress

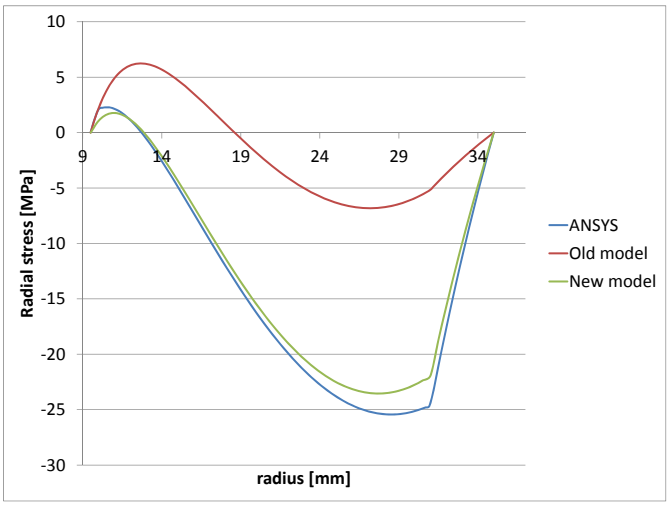

(b) radial stress

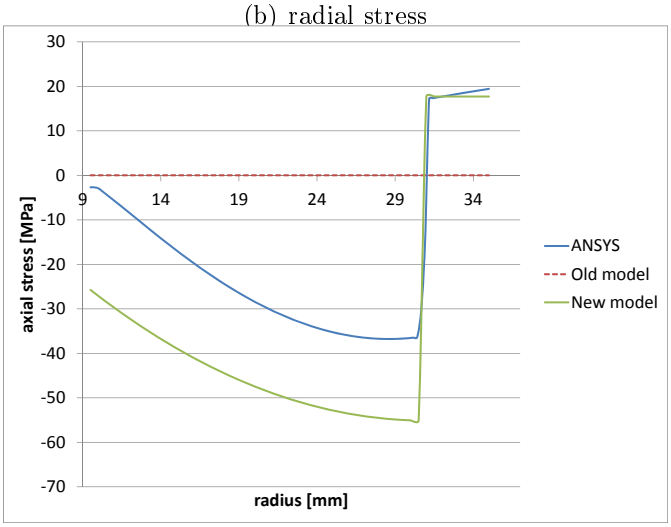

(c) axial stress

Figure 2.9: Detailed stresses in the self field solenoid

Chapter 3

Parametric analysis

3.1 Sensitivity to physical constants

It is important to estimate even the errors committed because of an inaccurate knowledge of physical parameters involved in mechanical calculations. In Figure 3.1 there are the normalized effects of the Young modulus of coil and skin, the Poisson ratio and the magnetic permeability on the peak hoop stresses both for coil and skin.

3.2 Effect of magnetic field

The magnetic field created by the solenoid itself depends on geometric parameters as demonstrated in 1.6 and in 1.7.

3.2.1 Self field configuration

Four different configurations were studied, as shown in Table 6.6. The inner radius ($R_1 = 9.5mm$), the length of the coil ($L_c = 126mm$) and the thickness of the skin ($t = 4mm$) were fixed, so the configurations were not

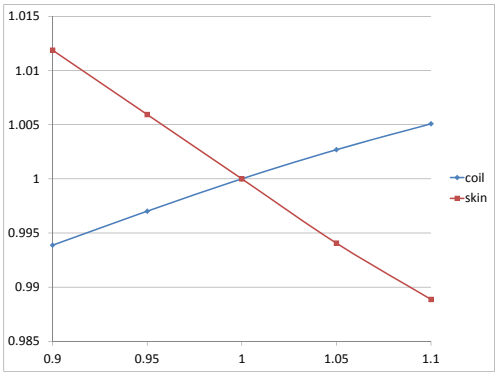

(a) coil Young modulus

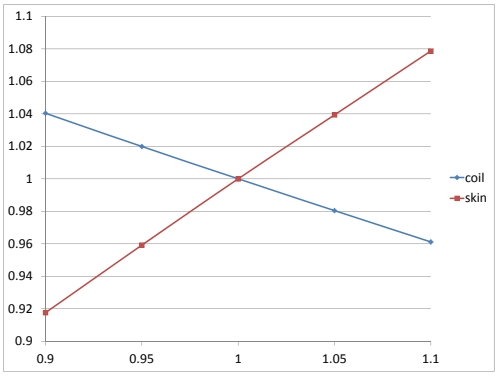

(b) skin Young modulus

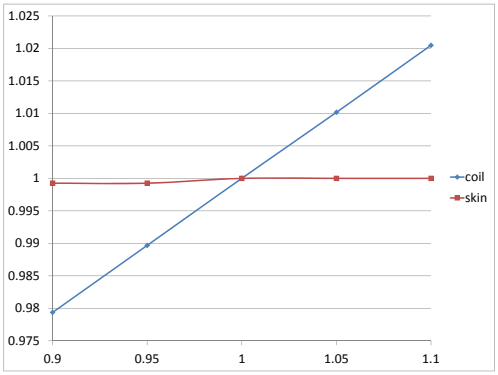

(c) coil Poisson ratio

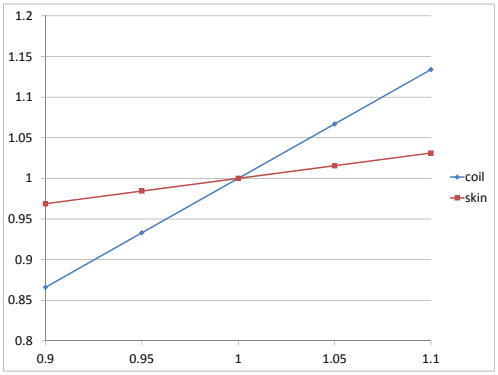

(d) magnetic permeability

Figure 3.1: Sensitivity to physical parameters

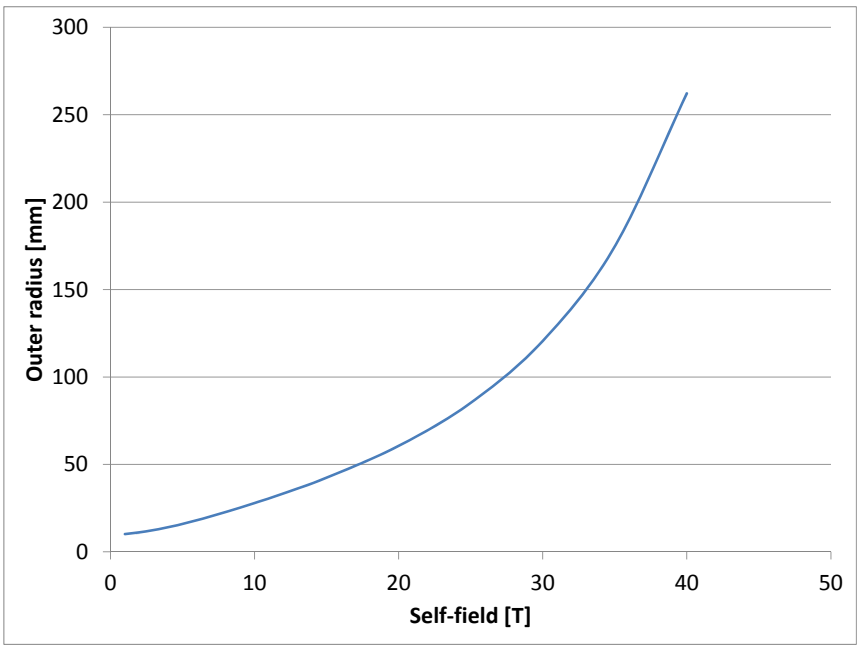

Figure 3.2: Outer radius

optimized in volume, according with RIFERIMENTO.

3.2.2 Insert coil configuration

An analysis was realized to determine the mechanical stresses of an insert coil loaded with a total magnetic field constant ($B_{tot} = 40T$) varying the geometry and the ratio between the self-field and the outer field. Four different configurations were studied, as shown in Table 3.2. The inner radius ($R_1 = 9.5mm$), the length of the coil ($L_c = 126mm$) and the thickness of the skin ($t = 4mm$) were fixed, so the configurations were not optimized in volume, according with RIFERIMENTO.

In Figure 3.5 there are the hoop stresses evaluated for the four configurations and compared with the behaviour of a self-field configuration with the same total magnetic field.

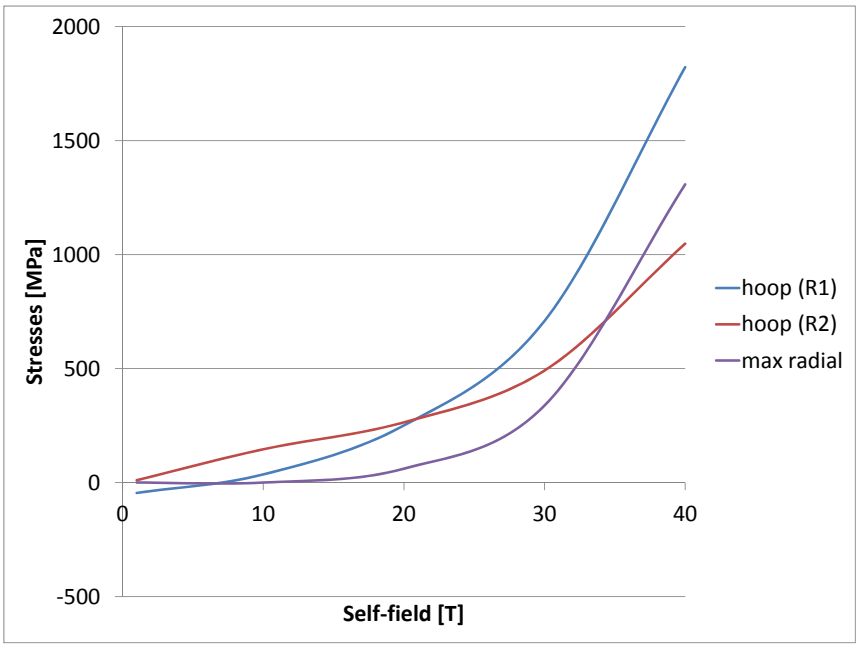

Figure 3.3: Stresses in the solenoid

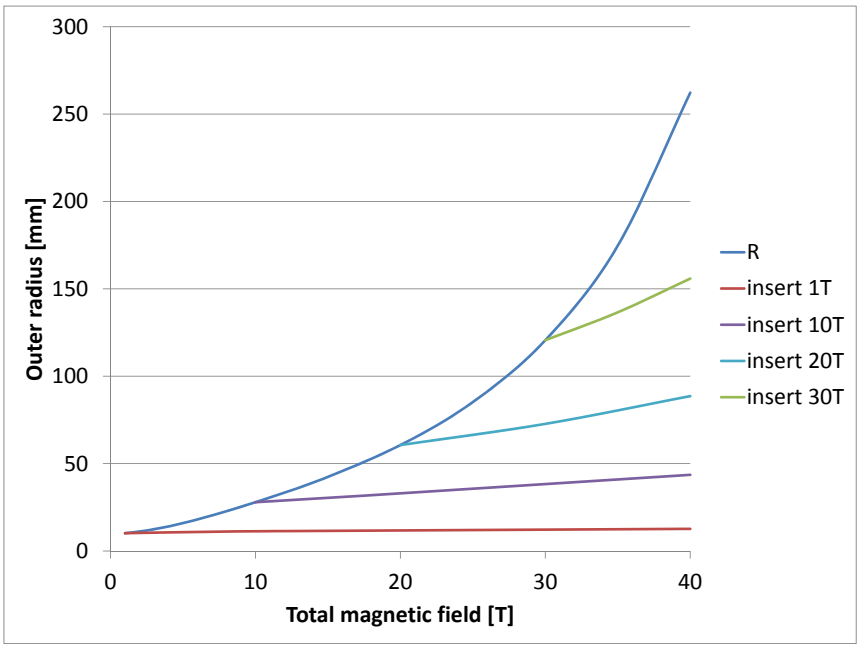

Figure 3.4: Outer radius in the insert coil

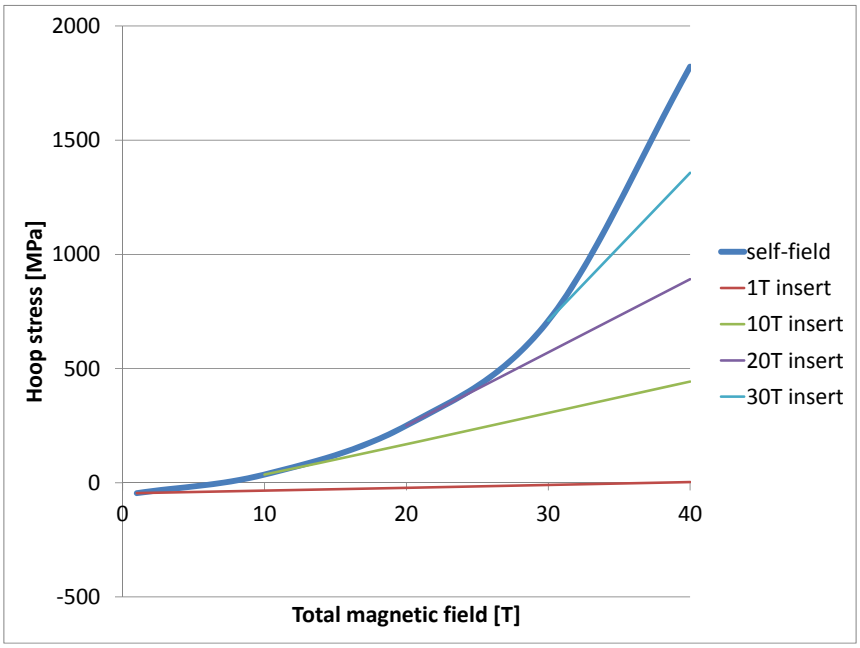

(a) coil

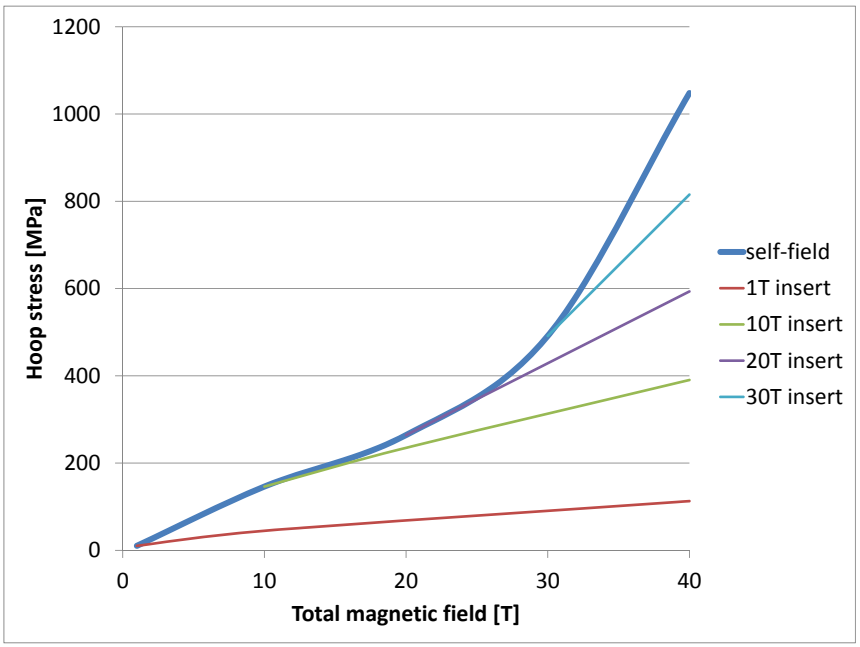

(b) skin

Figure 3.5: Hoop stresses in the insert coil

R_2	$B_{s.f.}$
$10.2mm$	$1T$
$27.9mm$	$10T$
$60.6mm$	$20T$
$120.6mm$	$30T$
$262.2mm$	$40T$

Table 3.1: Self-field configurations

R_2	$B_{s.f.}$	B_{out}
$12.7mm$	$1T$	$39T$
$43.6mm$	$10T$	$30T$
$88.6mm$	$20T$	$20T$
$155.9mm$	$30T$	$10T$

Table 3.2: Insert coil configurations

It very easy to understand that the two different load configurations doesn't produce the same mechanical effects in the solenoid. COMMENTI

3.3 Effects of geometric parameters

Usually the dimensions of the inner radius and the axial length of the solenoid are imposed, while the outer radius is determined by the self-field desired. In order to manage the stress distribution in the solenoid it is possible to change the skin thickness obtaining the effects shown in Figure 3.6.

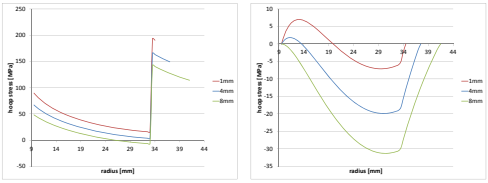

(a) hoop stress (b) radial stress

Figure 3.6: Effects of the skin thickness

3.4 Winding coil and assembly interference

3.4.1 Interference

In Figure 3.7 it is shown the linear dependence of the stresses on the interference between the coil and the skin at the assembly ($25C$) and working temperature ($4K$).

EFFETTO LINEARE : SOVRAPPOSIZIONE INTERFERENZA E TEMPERATURA

STRESS CON INTERFERENZE DIVERSE 3.8

3.4.2 Winding coil

The importance of winding coil can be easily understood if we consider a high field solenoid of $40T$ self-field and we compare the stresses of

3.4.3 Combination of effects

The task of minimizing stresses in the coil and in the skin can be reached considering both the effects of winding coil and assembly interference and superposing the solutions. In Figure 3.10, it is possible to see that there is a minimum of the hoop stress intensity in the coil. SPIEGARE MEGLIO PERCHE' POI INIZIA A CRESCERE DI NUOVO

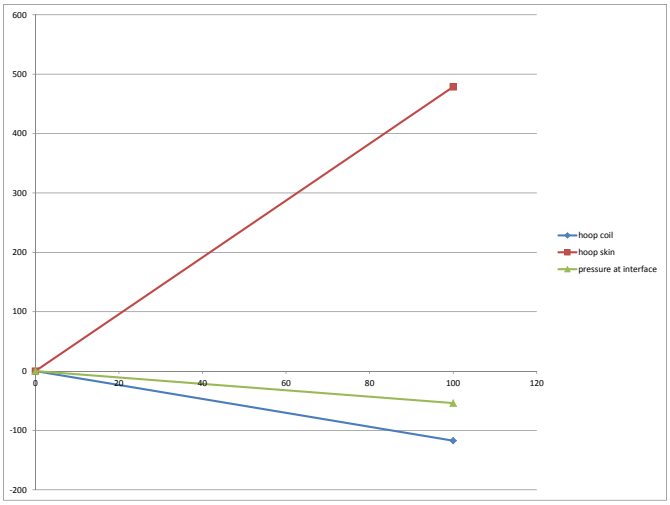

(a) $T = 25C$

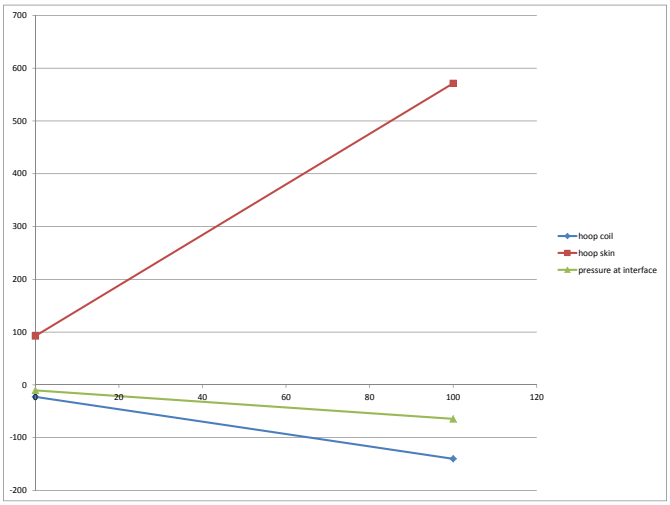

(b) $T = 4K$

Figure 3.7: Effects of interference on stresses at the assembly condition

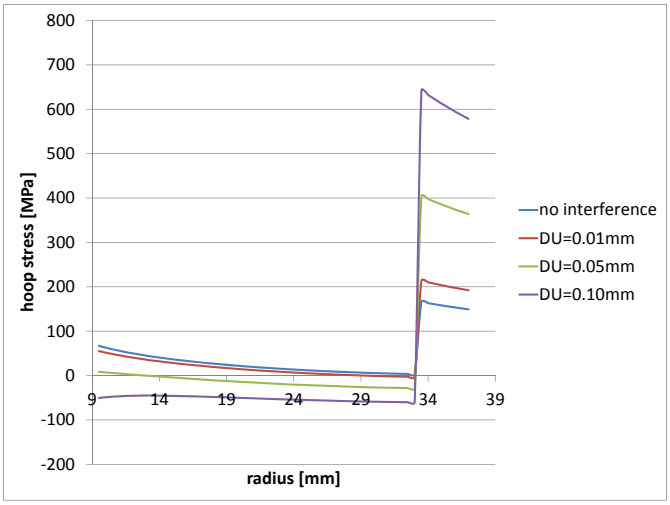

(a) hoop stress

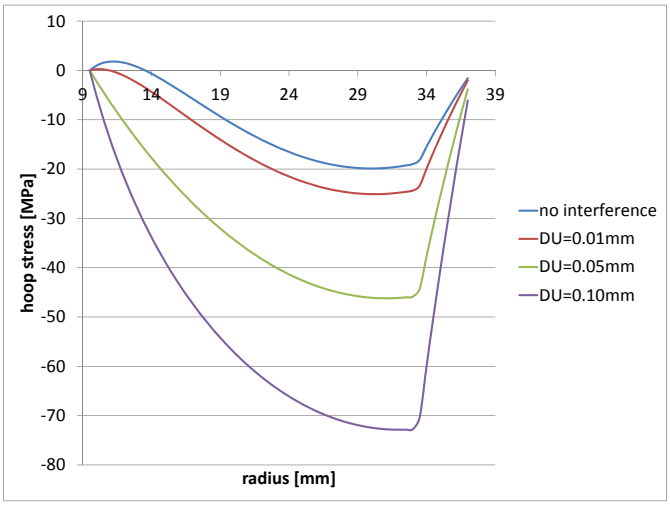

(b) radial stress

Figure 3.8: Effects of interference on stresses at the working condition

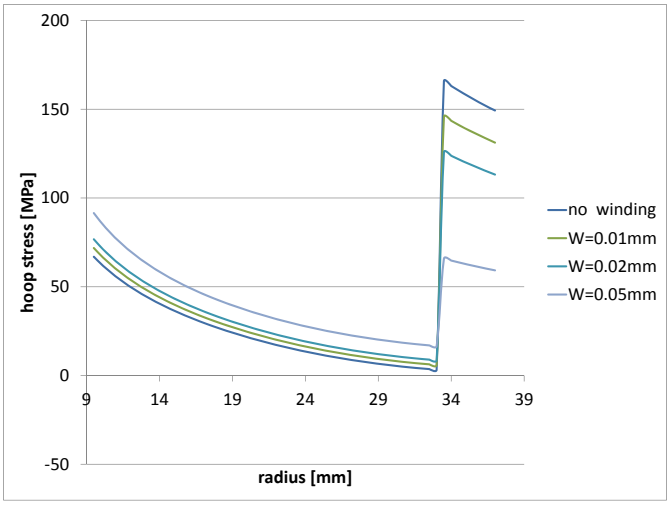

(a) hoop stress

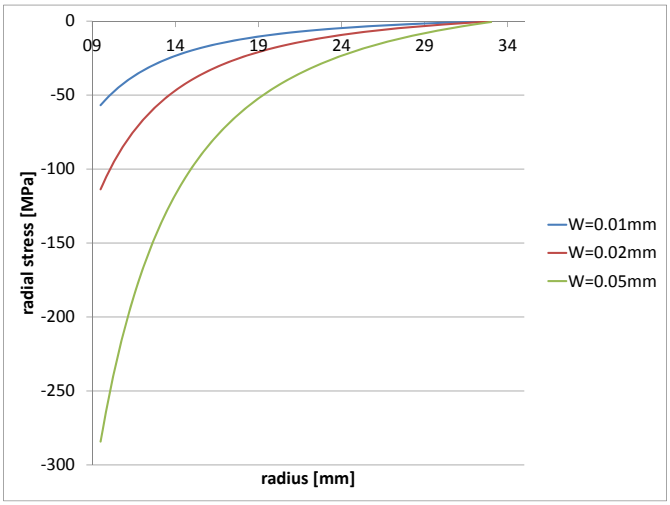

(b) radial stress

Figure 3.9: Effects of winding coil on stresses at the working condition

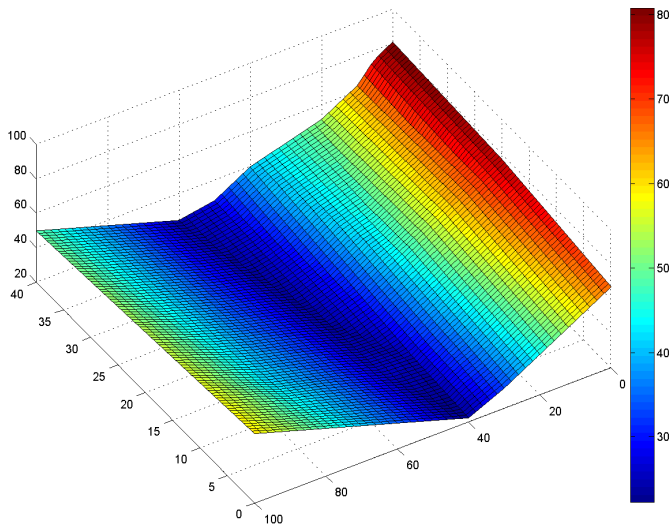

Figure 3.10: Hoop stres in the coil due to interference and winding

Chapter 4

Multiple skins configuration

4.1 Analytical model

In this new geometry, described in A.1 the same Lamé's equation 1.8 can be used to describe the mechanical behavior of the structure, but new boundary conditions are needed, in order to determine 8 independent coefficients.

$$
\begin{aligned}
\sigma_{rr,c_1}(R_1) &= 0 \\
\sigma_{rr,s_2}(R_2 + t_2) &= 0 \\
\sigma_{rr,c_1}(R_m) - \sigma_{rr,s_1}(R_m) &= 0 \\
\sigma_{rr,s_1}(R_m + t_1) - \sigma_{rr,c_2}(R_m + t_1) &= 0 \\
\sigma_{rr,c_2}(R_2) - \sigma_{rr,s_2}(R_2) &= 0 \\
u_{c_1}(R_m) - u_{s_1}(R_m) &= 0 \\
u_{s_1}(R_m + t_1) - u_{c_2}(R_m + t_1) &= 0 \\
u_{c_2}(R_2) - u_{s_2}(R_2) &= 0
\end{aligned}
$$

Even in this case the hypothesis that the magnetic load acts only on the

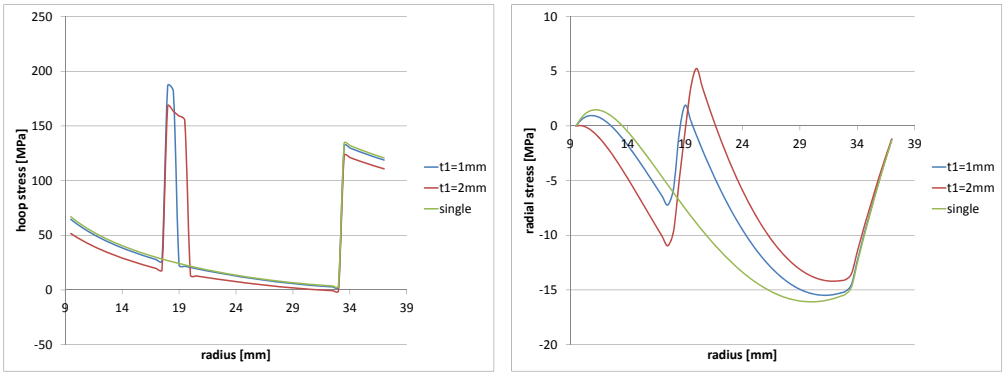

(a) hoop stress (b) hoop stress

Figure 4.1: Stress comparison

coil has been used. More over, the hypothesis of a linear behavior of the magnetic field was adopted neglecting the magnetic effect of a small steel skin between the two concentric coils.

The outer skin was considered to produce a background field for the inner one.

4.2 Results

4.3 Sensitivity to physical parameters

4.3.1 Magnetic field

To maximize the coil efficiency it was assumed that each coil section operates at its own minimum critical current density [7]. The inner coil has a critical current density lower than the outer one, so its outer radius can be varied to maximize the self-field of the double-coil. In Figure 4.3 is shown the total magnetic fields depending on R_m and on the thickness of the first skin. It is very easy to understand that it is possible to obtain an higher

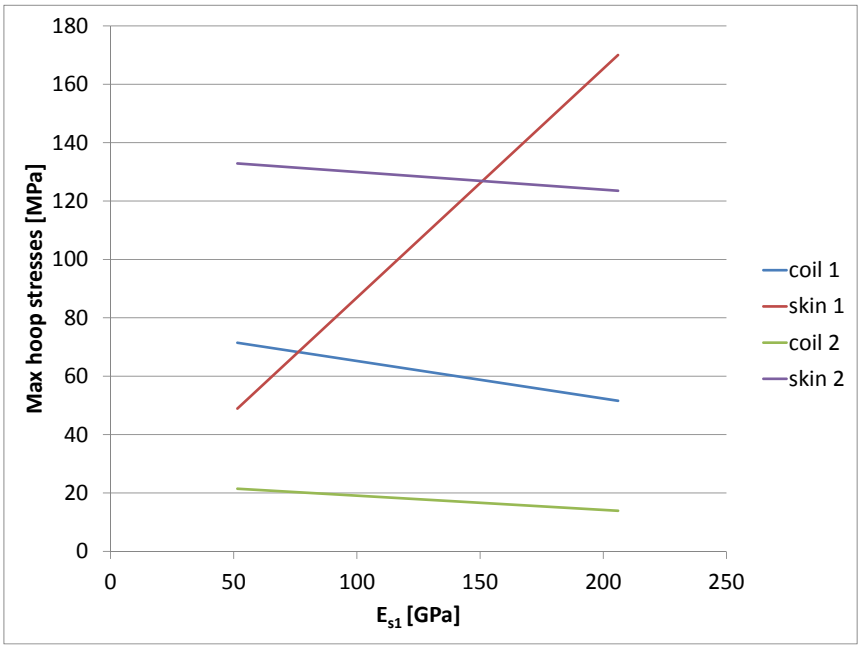

Figure 4.2: Maximum hoop stresses depending on the Young modulus of the inner skin

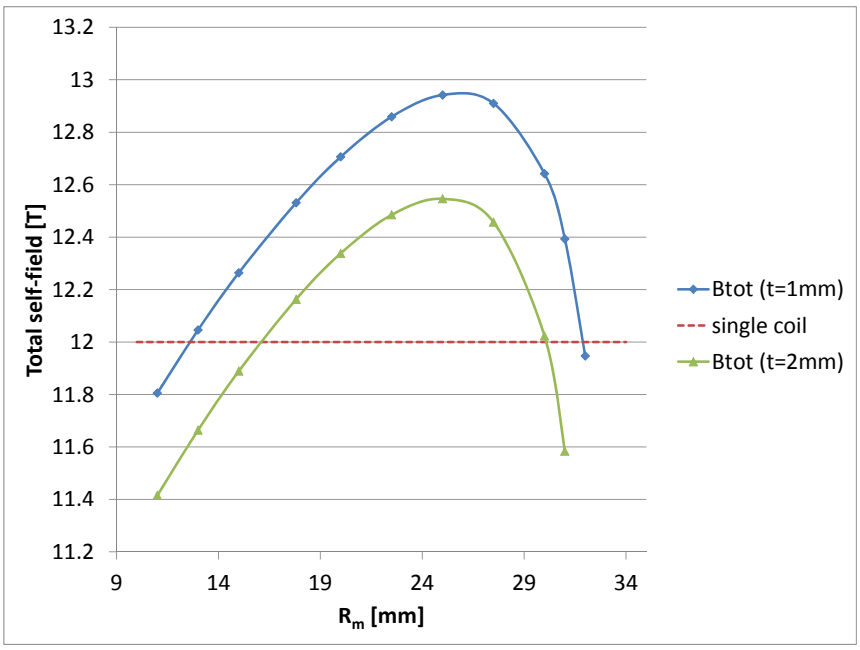

Figure 4.3: Total self-field depending on R_m

magnetic field with the same radial bulk.

Exploiting this important result, in Figure 4.4 it is shown the relationship between the total magnetic self-field on a single coil configuration and a double-coil configuration, where R_m was imposed to be the arithmetic average between R_1 and R_2. Just to have an idea of the possible material saving, for a $40T$ field the two outer radius are respectively $262mm$ and $198mm$ with a difference in volume of the 43%.

4.3.2 Geometrical optimization

In this configuration there are more geometrical parameters to set to design the solenoid, so it is possible to optimize better the combination of the effects in order to minimize stresses or to maximize the magnetic field.

In particular,

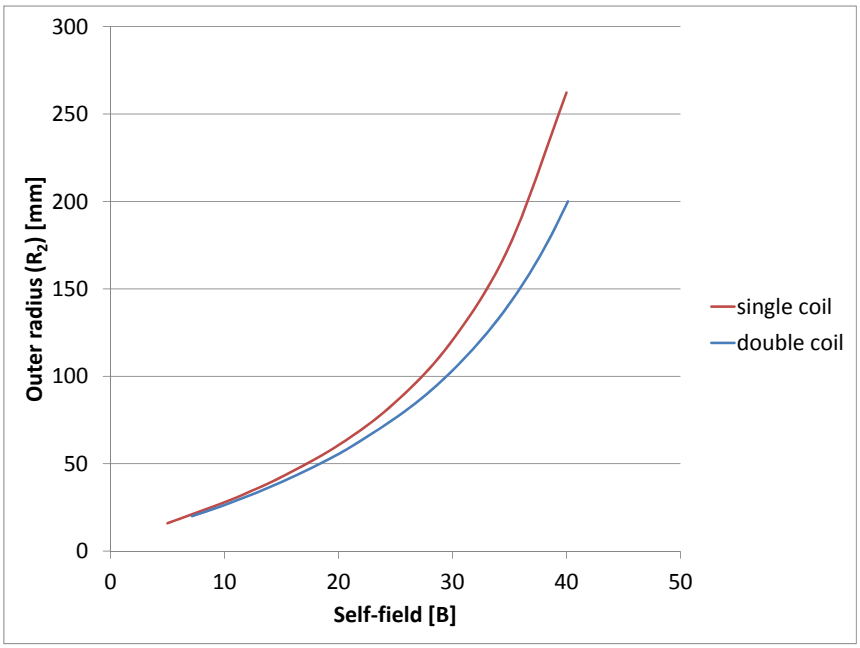

Figure 4.4: Outer radius

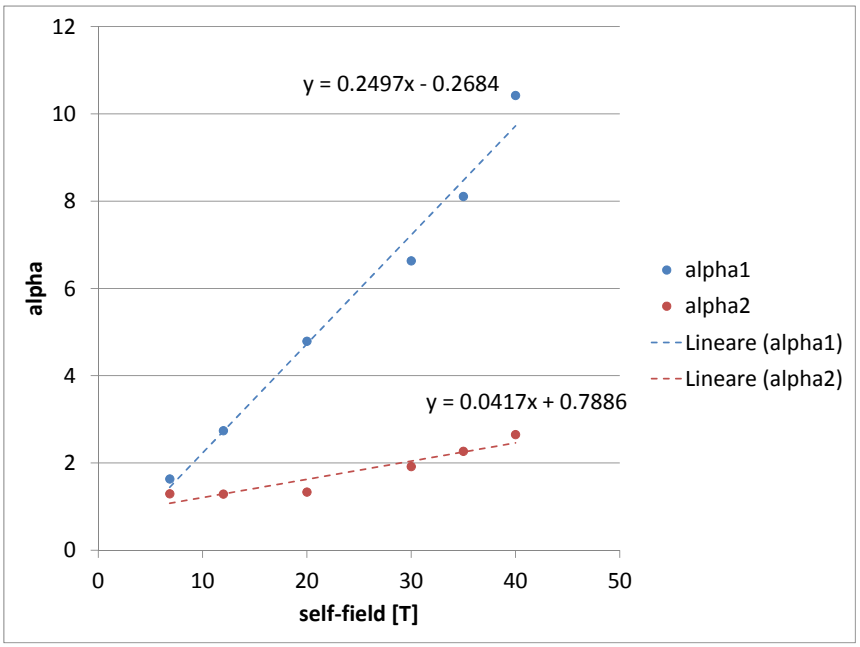

Figure 4.5: Optimized geometry

4.4 Discussion

Chapter 5

Applications of the analytic cal model

5.0.1 Estimate of the preload force

This model of the interference can be used to estimate the tension necessary to produce a fixed interference between the coil and the skin.

$$T_{skin} = \frac{\int_{R_2}^{R_2+t} \sigma_{\theta\theta,int}(r)dr}{N_{cables,skin}} \tag{5.1}$$

Considering the standard solenoid, in Figure **??** there is the relationship between the interference Δu and the preload tension T_{skin}.

RELAZIONE TRA DU E Fpreload

5.0.2 Estimate of the winding force

the medium tension necessary

$$T_{coil} = \frac{\int_{R_1}^{R_2} \sigma_{\theta\theta,int}(r)dr}{N_{cables,coil}} \tag{5.2}$$

where $N_{cable,coil} = \frac{L_c(R_2-R_1)}{4.5mm \cdot 0.125mm}$

Chapter 6

Case studies

This analytical model has been used to describe the magnetic behavior of three real configurations of solenoids used in the most important laboratories of the country:

- National High Magnetic Field Laboratory (NHMFL)
- Francis Bitter Magnet Laboratory at Massachusetts Institute of Technology (FBML-MIT)
- Brookhaven National Laboratory (BNL)

All the configurations studied were realized and tested taking into account almost only magnetic and electric parameters, but now it is possible even to consider analytically the mechanical behaviors and optimize the configurations.

6.1 National High Magnetic Field Laboratory

The coil Y10-3 was considered.

R_1	$7.15mm$
R_2	$19mm$
L_c	$100mm$

Table 6.1: NHMFL coil geometry

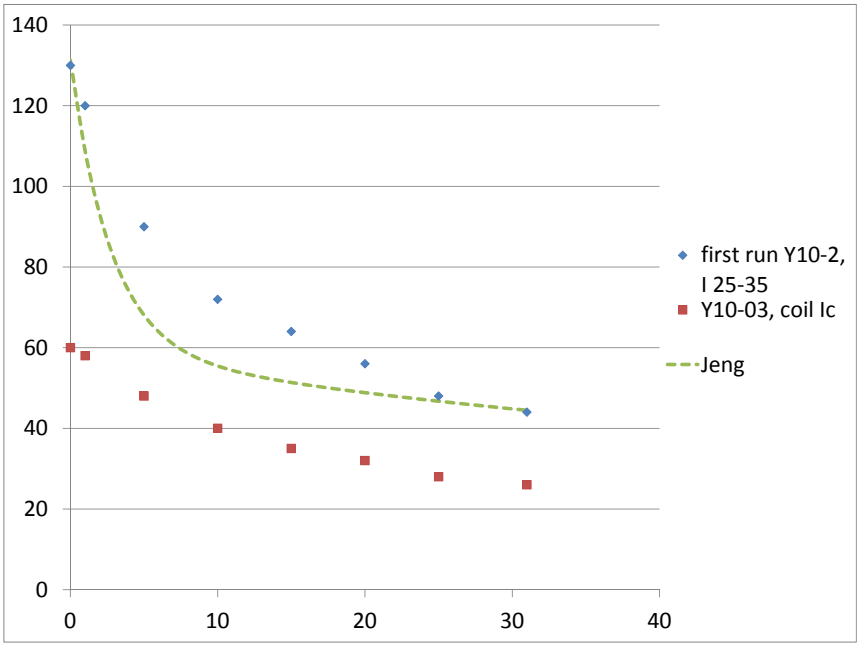

Figure 6.1: Critical current

6.1.1 Geometry

The coil Y10-3 was considered. The geometry is described in Table 6.1.

6.1.2 Critical current

Considering a tape width of $4.00mm$ and a thickness of $195.00\mu m$ and the Engineering Current Density calculated in 1.1.1, in Figure 6.1 are shown the experimental data obtained at NHMFL and our analytic distribution.

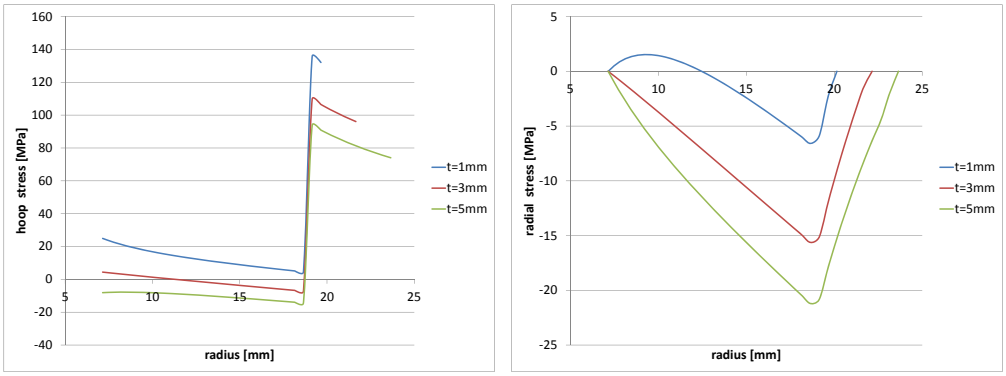

(a) hoop stress (b) hoop stress

Figure 6.2: Stress in NHMFL coil

6.1.3 Results

The configuration studied to calculate the mechanical stresses is the same used at NHMFL to determine the critical current, an insert coil with a background field of $31T$. The stresses obtained are shown in Figure 6.2.

6.2 Massachusetts Institute of Technologies

This configuration is a multiskin with two coils both realized in High Temperature Superconductors: the inner one is realized in YBCO while the outer is in Bi2223. The geometry and the materials properties are all listed in Tables 6.2 and 6.3.

6.2.1 Results

Considering the self-field loading configuration with the magnetic fields of Tables 6.2 and 6.3 the stresses obtained are shown in Figure 6.3. Three different skin configurations were considered in order to have a better idea of its influence on the mechanical behavior of the structure.

R_1	$74mm$
R_2	$142.3mm$
L_c	$462.2mm$
E_{YBCO}	$79.7GPa$
J	$19.94\frac{A}{mm^2}$
B_0	$8.33T$

Table 6.2: MIT insert 1

R_1	$158.3mm$
R_2	$221.3mm$
L_c	$518.2mm$
E_{Bi2223}	$106GPa$
J	$15.50\frac{A}{mm^2}$
B_0	$5.76T$

Table 6.3: MIT insert 2

The skin is very useful to reduce the hoop stress in the coil and, optimizing its thickness, it is even possible to control the max radial stress in the coil in order to avoid sliding among ropes. Both the configurations with an air interface and without have been considered emphasizing the different effects they produce in the distribution of stresses.

Actually, at Francis Bitter Magnet Laboratory the task is realizing lots of insert coils all concentric, so to have a better idea of the real stresses of the most loaded coils (the inner ones) the same geometry was loaded with a background magnetic field of $30T$ and the results are shown in Figure 6.4.

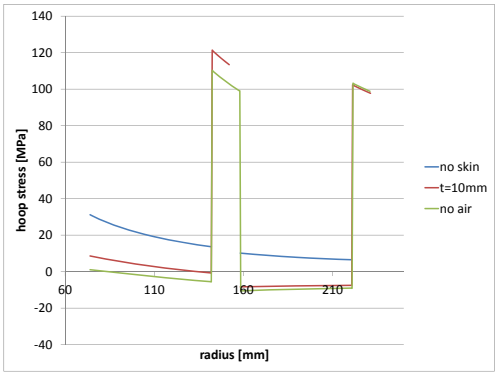

(a) hoop stress

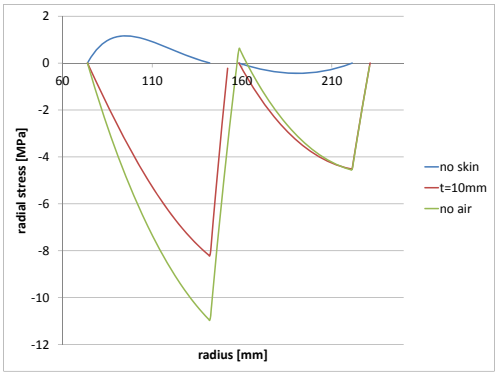

(b) hoop stress

Figure 6.3: Stress in MIT coil

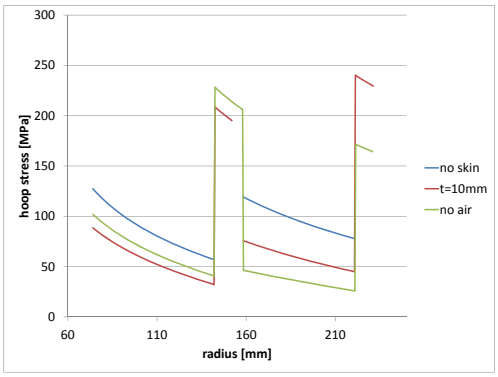

(a) hoop stress

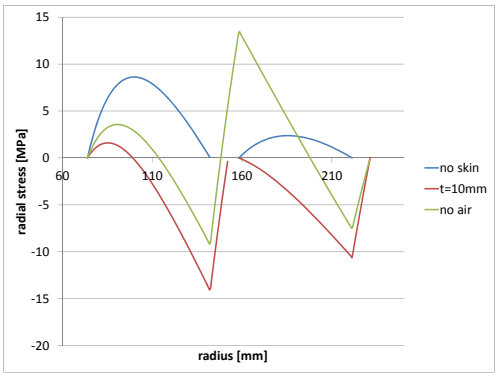

(b) hoop stress

Figure 6.4: Stress in MIT coil

R_1	$25mm$
R_2	$90mm$
L_c	$64mm$
B_0	$10T$

Table 6.4: Brookhaven insert 1

R_1	$100mm$
R_2	$160mm$
L_c	$128mm$
B_0	$12T$

Table 6.5: Brookhaven insert 2

6.3 Brookhaven National Laboratory

This last configuration was taken by the Brookhaven National Laboratory [?] among the geometries developed for muon colliders. Even in this case, the geometry is made of two concentric solenoids whose characteristics are described in Tables 6.4 and 6.5

6.3.1 Geometry

6.3.2 Results

Figure 6.5 shows the stresses of the two coils with no preload. We verified that, applying a 1 GPa inner-magnet banding pre-stress the resulting stresses agree with those obtained at Brookhaven National Laboratory as shown in Table **??**

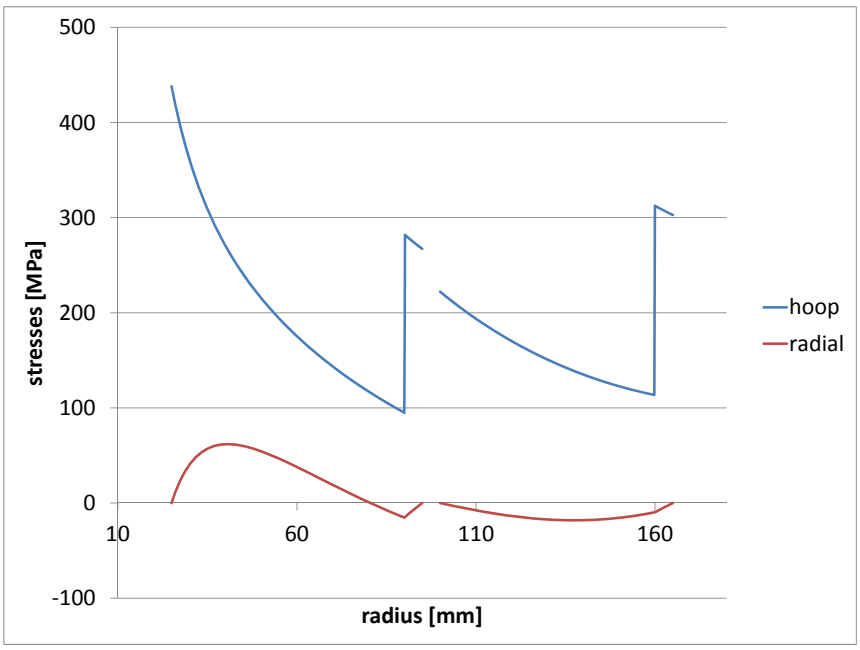

Figure 6.5: Stresses without pre-stress

	Fermilab	*Brookhaven*
max coil hoop stress	$327MPa$	$260MPa$
max skin hoop stress	$1.2GPa$	$1.1GPa$

Table 6.6: Self-field configurations

Bibliography

[1] Bartalesi A. Design of high field solenoids made of high temperature superconductors. MASTERS 04, FERMILAB, 2009.

[2] O. Belluzzi. *Scienza delle costruzioni.* Zanichelli, 1980.

[3] Wang-Z.J. Berman, G.J. Energy-minimizing kinematics in hovering insect flight. *Journal of Fluid Mechanics*, 582:153–168, 2007.

[4] Terzini E.; Barzi E. Analytical study of stress state in hts solenoids. Technical Report TM-2448-TD, FERMILAB, 2009.

[5] Brown G.V.; Flax L.; Itean E.C. Axial and radial magnetic fields of thick finite.length solenoids. Technical Report TN D-1993, NASA, 1963.

[6] Ekin J.W. *Experimental techniques for low-temperature measurements.* Oxford University Press, 2006.

[7] V.V. Kashikhin, E. Barzi, V.S. Kashikin, M. Lamm, Y. Sadovskiy, and A.V. Zlobin. Study of high field superconducting solenoids for muon beam cooling. *IGNOTO*, IGNOTO.

[8] Agrawal S.K. Khan, Z.A. Design and optimization of a biologically inspired flapping mechanism for flapping wing micro air vehicles. pages 373–378, 2007.

[9] Juvinall R.C.; Marshek K.M. *Fondamenti della progettazione dei componenti delle macchine.* ETS, 1993.

[10] Beghini M. *Dispense di Tecnica delle Costruzioni Meccaniche.* SEU Unipi, 2009.

[11] Zangheri S. Masutti, L. *Entomologia generale e applicata.* CEDAM.

[12] Wilson M.N. *Superconducting Magnets.* Oxford Science Publications, 1983.

[13] Woinowski-Krieger S. Timoshenko, S. *Theory of plates and shells.* McGraw Hill, 1959.

Appendix A

Definition of the standard solenoid

CARATTERISTICHE

A.1 Double coil

Appendix B

Materials properties

Material	$\alpha(10^{-6}K^{-1})$
Steel	10
YBCO	8
BSCCO	14.5
Copper	16.7
G10	????

Table B.1: Coefficients of thermal dilatation

Appendix C

Mathcad code

Parametri dei materiali

$E_c := 79.7GPa$

$ni_c := 0.3$

$E_s := 206GPa$

$ni_s := 0.3$

$mu_0 := 4 \cdot \pi \cdot 10^{-7} T \cdot \frac{m}{A}$

$a_{cT} := 8 \cdot 10^{-6} K^{-1}$

$a_{sT} := 10 \cdot 10^{-6} K^{-1}$

Densità di corrente critica

$c_1 := 1018 \frac{A}{mm^2}$

$c_2 := -0.3606 T^{-1}$

$c_3 := 503.3 \frac{A}{mm^2}$

$c_4 := -0.01702 T^{-1}$

$J_c(B_{tot}) := c_1 \cdot \exp(c_2 \cdot B_{tot}) + c_3 \cdot \exp(c_4 \cdot B_{tot})$

Caratteristiche geometriche

$t := 4mm$

Effetti termici e interferenze

$DT := -290K$

$DU := 0 \cdot 10^{-3} mm$

$DU_{coil} := 0 \cdot 10^{-3} mm$

$R_1 := 9.5mm$

$R_2 := 25mm$

$L_c := 126mm$

Campi magnetici

$B_{selffield} := 10T$

$B_{infield} := 0T$

$B_{tot} := B_{selffield} + B_{infield}$

$B_{tot} = 10\,T$

Densità corrente

$J_c(B_{tot}) = 4.522 \times 10^8 \frac{A}{m^2}$

IN ANSYS

$costante := 1$

$J_{eng}(B_{tot}) := \frac{J_c(B_{tot})}{costante}$

$alpha(R_1, R_2) := \frac{R_2}{R_1}$

$beta(R_1, L_c) := \frac{L_c}{2} \cdot \frac{1}{R_1}$

$$B_0(R_1,R_2,L_c) := J_{eng}(B_{tot})\cdot\left(R_1\cdot mu_0\cdot beta(R_1,L_c)\cdot\ln\left(\frac{\sqrt{alpha(R_1,R_2)^2 + beta(R_1,L_c)^2} + alpha(R_1,R_2)}{\sqrt{1 + beta(R_1,L_c)^2} + 1}\right)\right)$$

Given

$$B_0(R_1,R_2,L_c) = B_{selffield}$$

$$R_2 := Find(R_2)$$

$$R_2 = 2.7903\times 10^{-2}\,m$$

$$R_2 := 33.39242mm$$

bisogna ridefinire R.2 (non so perché) !!!

$$B_0(R_1,R_2,L_c) = 12.805\,T$$

Modello meccanico

$$u_c(r,C_1,C_2) := \frac{-\left(1 - ni_c^{\,2}\right)\cdot J_{eng}(B_{tot})}{E_c}\cdot\left[\frac{B_0(R_1,R_2,L_c)}{(R_2 - R_1)}\left(\frac{R_2\cdot r^2}{3} - \frac{r^3}{8}\right) + B_{infield}\cdot\frac{r^2}{3}\right] + C_1\cdot r + \frac{C_2}{r} \rightarrow$$

$$e_{c.hoop}(r, C_1, C_2) := \frac{u_c(r, C_1, C_2)}{r} \rightarrow$$

$$e_{c.radial}(r, C_1, C_2) := \frac{d^1}{dr^1} u_c(r, C_1, C_2) \rightarrow$$

$$u_{c.int}(r, C_1, C_2) := \left(C_1 \cdot r + \frac{C_2}{r}\right) \rightarrow$$

$$e_{c.hoop.int}(r, C_1, C_2) := \frac{u_{c.int}(r, C_1, C_2)}{r} \rightarrow$$

$$e_{c.radial.int}(r, C_1, C_2) := \frac{d^1}{dr^1} u_{c.int}(r, C_1, C_2) \rightarrow$$

$$s_{c.hoop.int}(r, C_1, C_2) := \frac{E_c}{1 - ni_c^{\,2}} \cdot \left(e_{c.hoop.int}(r, C_1, C_2) + ni_c \cdot e_{c.radial.int}(r, C_1, C_2)\right) \rightarrow$$

$$s_{c.radial.int}(r, C_1, C_2) := \frac{E_c}{1 - ni_c^{\,2}} \cdot \left[\left(e_{c.radial.int}(r, C_1, C_2) \right) + ni_c \cdot \left(e_{c.hoop.int}(r, C_1, C_2) \right) \right] \rightarrow$$

$$C_1 := 1$$

$$C_2 := 1mm^2$$

Given

$$s_{c.radial.int}(R_2, C_1, C_2) = 0$$

$$u_{c.int}(R_1, C_1, C_2) = DU_{coil}$$

$$\begin{pmatrix} C_{1int} \\ C_{2int} \end{pmatrix} := \mathrm{Find}(C_1, C_2) \rightarrow$$

$$s_{s.hoop.int}(r, C_{1int}, C_{2int}) \rightarrow$$

$$s_{c.radial.int}(r, C_{1int}, C_{2int}) \rightarrow$$

$$s_{c.hoop}(r, C_1, C_2) := \frac{E_c}{1 - ni_c^{\,2}} \cdot \left[\left(e_{c.hoop}(r, C_1, C_2) - a_{cT} \cdot DT \right) + ni_c \cdot \left(e_{c.radial}(r, C_1, C_2) - a_{cT} \cdot DT \right) \right] + s_{c.hoop.int}(r, C_{1int}, C_{2int}) \rightarrow$$

$$s_{c.radial}(r, C_1, C_2) := \frac{E_c}{1 - ni_c^{\,2}} \cdot \left[\left(e_{c.radial}(r, C_1, C_2) - a_{cT} \cdot DT \right) + ni_c \cdot \left(e_{c.hoop}(r, C_1, C_2) - a_{cT} \cdot DT \right) \right] + s_{c.radial.int}(r, C_{1int}, C_{2int}) \rightarrow$$

Skin

$$u_s(r, D_1, D_2) := \left(D_1 \cdot r + \frac{D_2}{r} \right) \rightarrow$$

$$e_{s.hoop}(r, D_1, D_2) := \frac{u_s(r, D_1, D_2)}{r} \rightarrow$$

$$e_{s.radial}(r, D_1, D_2) := \frac{d^1}{dr^1} u_s(r, D_1, D_2) \rightarrow$$

$$s_{s.hoop.int}(r, D_1, D_2) := \frac{E_s}{1 - ni_s^{\,2}} \cdot \left(e_{s.hoop}(r, D_1, D_2) + ni_s \cdot e_{s.radial}(r, D_1, D_2) \right) \rightarrow$$

$$s_{s.radial.int}(r, D_1, D_2) := \frac{E_s}{1 - ni_s^2} \cdot \left[\left(e_{s.radial}(r, D_1, D_2) \right) + ni_s \cdot \left(e_{s.hoop}(r, D_1, D_2) \right) \right] \rightarrow$$

$$D_1 := 1$$

$$D_2 := 1mm^2$$

Given

$$s_{s.radial.int}(R_2 + t, D_1, D_2) = 0$$

$$u_s(R_2, D_1, D_2) = DU$$

$$\begin{pmatrix} D_{1int} \\ D_{2int} \end{pmatrix} := \mathrm{Find}(D_1, D_2) \rightarrow$$

$$s_{s.hoop.int}(r, D_{1int}, D_{2int}) \rightarrow$$

$$s_{s.radial.int}(r, D_{1int}, D_{2int}) \rightarrow$$

$$s_{s.hoop}(r, D_1, D_2) := \frac{E_s}{1 - ni_s^2} \cdot \left[\left(e_{s.hoop}(r, D_1, D_2) - a_{sT} \cdot DT \right) + ni_s \cdot \left(e_{s.radial}(r, D_1, D_2) - a_{sT} \cdot DT \right) \right] + s_{s.hoop.int}(r, D_{1int}, D_{2int}) \rightarrow$$

$$s_{s.radial}(r, D_1, D_2) := \frac{E_s}{1 - ni_s^2} \cdot \left[\left(e_{s.radial}(r, D_1, D_2) - a_{sT} \cdot DT \right) + ni_s \cdot \left(e_{s.hoop}(r, D_1, D_2) - a_{sT} \cdot DT \right) \right] + s_{s.radial.int}(r, D_{1int}, D_{2int}) \rightarrow$$

Condizioni al contorno

$C_1 := 1$ $\qquad$ $D_1 := 1$

$C_2 := 1mm^2$ $\qquad$ $D_2 := 1mm^2$

Given

$$s_{c.radial}(R_1, C_1, C_2) = 0$$

$$s_{s.radial}(R_2 + t, D_1, D_2) = 0$$

$$s_{c.radial}(R_2, C_1, C_2) = s_{s.radial}(R_2, D_1, D_2)$$

$$u_c(R_2, C_1, C_2) = u_s(R_2, D_1, D_2)$$

$$\begin{pmatrix} C_{1sf} \\ C_{2sf} \\ D_{1sf} \\ D_{2sf} \end{pmatrix} := \mathrm{Find}(C_1, C_2, D_1, D_2) \rightarrow$$

$$s_{hoop}(r) := \begin{cases} s_{c.hoop}(r, C_{1sf}, C_{2sf}) & \text{if } r < R_2 \\ s_{s.hoop}(r, D_{1sf}, D_{2sf}) & \text{otherwise} \end{cases}$$

$$s_{radial}(r) := \begin{cases} s_{c.radial}(r, C_{1sf}, C_{2sf}) & \text{if } r < R_2 \\ s_{s.radial}(r, D_{1sf}, D_{2sf}) & \text{otherwise} \end{cases}$$

$$u(r) := \begin{cases} u_c(r, C_{1sf}, C_{2sf}) & \text{if } r < R_2 \\ u_s(r, D_{1sf}, D_{2sf}) & \text{otherwise} \end{cases}$$

$$s_{c.axial.p}(r) := ni_c \cdot \left(s_{c.hoop}(r, C_{1sf}, C_{2sf}) + s_{c.radial}(r, C_{1sf}, C_{2sf})\right) \rightarrow$$

$$s_{s.axial.p}(r) := ni_s \cdot \left(s_{s.hoop}\left(r, D_{1sf}, D_{2sf}\right) + s_{s.radial}\left(r, D_{1sf}, D_{2sf}\right)\right) \rightarrow$$

$$s_{c.axial.m} := \frac{\int_{R_1}^{R_2} s_{c.axial.p}(r)\, dr}{R_2 - R_1} =$$

$$s_{s.axial.m} := \frac{\int_{R_1}^{R_2} s_{s.axial.p}(r)\, dr}{R_2 - R_1} =$$

$$I := J_{eng}\left(B_{tot}\right) \cdot (0.45 \cdot 0.125)\, mm^2 = 25.435\, A$$

SISTEMARE

$$B_r := 3T$$

$$B_r = 3\, T$$

$$F_{axial} := B_r \cdot I \cdot \pi \cdot \left(R_1 + R_2\right)$$

$$F_m := \int_{R_1}^{R_2} B_r \cdot J_{eng}\left(B_{tot}\right) \cdot 2\pi \cdot r^2\, dr$$

$$s_{axial.mag} := \frac{F_m}{\pi\left(R_2^{\,2} - R_1^{\,2}\right)}$$

$$s_{c.axial}(r) := s_{c.axial.p}(r) - s_{c.axial.m} - s_{axial.mag}$$

$$s_{s.axial}(r) := s_{s.axial.p}(r) - s_{s.axial.m}$$

$$s_{axial}(r) := \begin{cases} s_{c.axial}(r) & \text{if } r < R_2 \\ s_{s.axial}(r) & \text{otherwise} \end{cases}$$

Forze di preload

$$F_{skin} := L_c \cdot \int_{R_2}^{R_2+t} s_{s.hoop.int}(r, D_{1int}, D_{2int})\, dr$$

$$F_{coil} := L_c \cdot \int_{R_1}^{R_2} s_{c.hoop.int}(r, C_{1int}, C_{2int})\, dr$$

$$N_{cavi.coil} := \frac{L_c \cdot (R_2 - R_1)}{4.5mm \cdot 0.125mm} = 5.352 \times 10^3$$

$$r_{cable} := 1mm$$

$$N_{cavi.skin} := \frac{L_c}{2 \cdot r_{cable}} \cdot \frac{t}{2 \cdot r_{cable}} = 126$$

$$T_{coil} := \frac{F_{coil}}{N_{cavi.coil}}$$

$$T_{skin} := \frac{F_{skin}}{N_{cavi.skin}}$$